Applied Thermal Engineering 302 (2026) 131728

Contents lists available at ScienceDirect

Applied Thermal Engineering

journal homepage: www.elsevier.com/locate/ate

Research Paper

Advancing simultaneous component and cycle optimization: A holistic cycle-optimized collaborative design concept for Brayton cycle heat pumps

Jens Gollasch [a,*], Michael Lockan [b]

[a] German Aerospace Center, Institute of Low-Carbon Industrial Processes, Simulation and Virtual Design, Weinbergstr. 10, Cottbus, 03050, Brandenburg, Germany
[b] German Aerospace Center, Institute of Low-Carbon Industrial Processes, High Temperature Heat Pumps, Weinbergstr. 10, Cottbus, 03050, Brandenburg, Germany

ARTICLE INFO

Keywords:
Brayton cycle heat pump
Holistic optimization
Integrated compressor design
Cycle optimization
Heat exchanger design

ABSTRACT

To achieve globally optimal performance of industrial heat pumps, matching both thermodynamic cycle and component parameters is a complex challenge. The integration of multiple disciplines and design stages is required. Holistic design strategies, which simultaneously optimize thermodynamic cycle parameters together with detailed component optimizations are able to overcome the shortcomings of conventional sequential design. However, the complexity significantly increases with high dimensionality integrating all disciplinary analyses. Four optimization architectures are analyzed, integrating multi-stage compressor optimization and heat exchanger sizing with cycle optimization. Distributed structures that solve the component subproblems separately, yield higher reliability, better objectives, and faster convergence, though at increased computational cost. Surrogate models trained with active learning strategies are able to reduce function evaluations enabling integration of complex models. A collaborative optimization concept with distributed cycle optimization is identified as the most effective, achieving convergence in fewer than 500 evaluations and designing a Brayton cycle heat pump with a COP of 1.82 at a 260 K temperature lift. The trade-off with engine size is demonstrated in a multi-objective approach highlighting the potential of holistic optimizations for high-temperature heat pumps.

1. Introduction

The design process of industrial heat pumps (HP) is a complex challenge with the objective to find the globally optimal performance while matching both thermodynamic cycle and component parameters. High temperature heat pumps will play a major role to electrify process heat and have been identified as a key technology for decarbonization with the need for further demonstration of the technology [1–3]. Brayton heat pumps with high temperature lifts are novel technologies that can potentially be used for high temperature applications, drying processes or pumped thermal storage [4–6]. Frate et al. [7] investigated the impact of compressor designs for the Brayton cycle finding feasible single stage configurations with sink temperatures up to 350°C. Heat pumps depend very much on the efficiency of their components. Several disciplinary analyses and fidelity-levels with varying modeling-depths need to be considered. The conventional design process is usually an sequential procedure which can be of high effort and very time consuming. Fundamental decisions are usually made during the conceptual phase of cycle design. In the following steps, matching component designs are developed with increasing level of detail. The components need to be matched on cycle level, which leads to an iterative procedure. One major shortcoming of conventional design is the fact, that important decisions have to be made without knowing the exact performance capabilities of the components like turbomachines and heat exchangers. This means, that assumptions have to be made in earliest phases of design. This can lead to trial-and-error while mistakes made in cycle conceptualization will propagate through the design process and are hard to revert in the following steps. This sequential procedure makes it impossible to achieve a globally optimal heat pump, where each component is matched to perform in its best design point with regard to the overall engine efficiency.

The concept of holistic heat pump design is able to mitigate these issues as thermodynamic cycle and components are optimized simultaneously. Especially in closed cycles, the component performance parameters are highly interactive and matching on cycle level is of major importance. For holistic design, detailed physics based analyses of the components are integrated in a single design process. In case of heat pump design, this can include aerodynamic modeling of turbomachines as well as heat transfer and pressure drop simulations of heat exchangers. Interfaces between all disciplines are defined to

* Corresponding author.
E-mail address: jens.gollasch@dlr.de (J. Gollasch).

https://doi.org/10.1016/j.applthermaleng.2026.131728
Received 28 March 2026; Received in revised form 15 May 2026; Accepted 30 May 2026
Available online 6 June 2026

Nomenclature

Acronyms

AAO	All-at-once optimization
CD	Collaborative optimization
GPR	Gaussian process regression
HEX, HE	Heat exchanger
HTHP	High temperature heat pump
LHS	Latin hypercube sampling
MDO	Multi-disciplinary optimization
NHX	Nested heat exchanger design
OCD	Cycle optimized collaborative optimization
PC	Process chain
RS	Response surface
SLC	Streamline curvature
ttd	Terminal temperature difference

Latin symbols

$\boldsymbol{c}$	Constant parameter vector
$\boldsymbol{h}$	Constraint vector
$\boldsymbol{p}$	Design vector
$\boldsymbol{s}$	Station value vector
$\boldsymbol{y}$	Output vector of analyses
$\dot{m}$	Mass flow [kg/s]
$\dot{Q}$	Heat flow rate [W]
$\dot{W}$	Power [W]
$\mathcal{N}$	Gaussian distribution
COP	Coefficient of performance [–]
e_a	Approximation error
l	length [m]
n	Number of
P	Total pressure [Pa]
R	Radius [m]
R^2	Coefficient of determination
$s_{1,2}$	Tube separation
T	Temperature [K]
ttd	Terminal temperature difference

Greek symbols

α	Taper angle [°]
β	Outflow angle [°]
ζ	Tolerance vector
δ	Deviation from target value
η	Isentropic efficiency [–]
ω	Rotational speed [1/min]
Π	Pressure ratio [–]
σ	Standard deviation

Superscripts and subscripts

$*$	Optimized value
$\hat{}$	Target value
$\tilde{}$	Predicted value
B	Baffles, blades
C	Compressor
cyc	Cycle
h	Hub
H, HTHX	Heat sink heat exchanger
L, LTHX	Heat source heat exchanger
R	Recuperator
s	shell
T	Turbine
t	tubes

formulate the holistic optimization problem. Depending on the integrated methods and their dimensions, the complexity can largely increase. Holistic optimization problems are thereby difficult to solve. But in comparison to sequential design, a successful implementation of a holistic optimization strategy will balance cycle parameters and component performance for maximized efficiency. Another advantage is that geometric information is available throughout the design process, so that additional objectives like engine size, weight or costs can be considered.

1.1. State of the art: Holistic optimization

In the field of multi-disciplinary optimization (MDO) some general concepts for holistic system optimization have been introduced. In most cases they are investigated with reduced problems and only few have been fully implemented for detailed design processes. The challenge of MDO problems is to deal with local parameters of individual disciplines (components) and orchestrate the overall system optimization with the exchange of interface parameters. In this way, the interactions of all subproblems can be considered which allows to find the globally optimal system. Additionally, solving these kind of problems will improve the coordination between involved individuals, departments or companies and thereby make the entire design process more efficient considering time and costs.

Martins et al. [8] compared and classified several architectures for MDO problems. They distinguish between monolothic structures, that solve a single optimization problem (e.g. all-at-once optimization AAO) and distributed structures, that introduce subproblem optimization. For the distributed problems, they considered (among others) concurrent-subspace optimization (CSSO), collaborative optimization (CO), Bilevel Integrated System Synthesis (BLISS) and Analytical Target Cascading (ATC). They conclude that there is a high demand for further research to benchmark these architectures. Braun et al. [9] introduced the concept of CO and there are several studies with further developments and investigations concerning its performance [10–12]. The optimization is split up into a master problem and subproblems for each discipline. Sobieski and Kroo [13] introduced the integration of response surfaces (RS) in CO structures to improve the performance. Response surfaces are computationally inexpensive, which is important as the subproblems have to be solved numerous times. They applied quadratic RS for a test problem that is solved with a trust region approach. Integrated approaches for cycle design have been performed in the field of aero-engines, organic Rankine cycles (ORC) and heat pumps. Tacconi et al. [14] applied an holistic approach to the design of a semi-closed engine cycle of a propulsion system. They coupled fast methods of component sizing with overall system design to minimize fuel consumption and engine weight. Hendler et al. [15] compared two optimization concepts for coupled multi-stage compressor and combustor design. Both investigated holistic concepts improve designs concerning fuel consumption and efficiency with an AAO architecture delivering the best results. System level parameters remain unchanged. Another field of applied MDO is the design of organic Rankine cycles. There are several studies that integrate meanline turbine design with the optimization of the thermodynamic cycle [16–18]. Integrated design leads to improvements and time effort of the design process can be significantly reduced. Schuster et al. demonstrate that integrating mean-line radial turbine model into ORC system optimization, including multi-stage turbine designs for higher pressure ratios, enables high cycle efficiency [19]. For heat pump design, most studies focus on the integration of compressor meanline analysis: Meroni et al. [20] maximized cycle performance and heat flow rate for different working fluids by integration of a meanline based radial compressor design. Giuffre et al. [21] used a surrogate model for fast evaluation of integrated radial compressor analysis to speed up the multi-objective optimization process. An artificial neural network (ANN) is trained to predict the compressor performance. They continued their work in [22] and balanced system weight and power consumption, specifically through the design of the evaporator in a multi-point approach. Ascione et al. [23] also applied integrated system optimization to investigate the trade-off between engine weight and performance. Advantages of integrated design are highlighted and computational costs are kept moderate by using parameter reduction. Altogether, 57,600 function evaluations lead to convergence for 24 variables Three design approaches are compared by Beltrame et al. [24] where two are integrated approaches with one using a surrogate to predict optimal condensers. Integrated design improves the performance and the surrogates reduce computational effort. Schaffrath et al. [25] evaluated the CFD based design of radial steam compressors in a 2-stage cycle configuration of a reversed Rankine cycle. Convergence has been improved by using a multi-fidelity (co-Kriging) approach for the optimization. Yan et al. [26] have integrated a mean-line compressor analysis that links the thermodynamic cycle optimization to the aerodynamic compressor performance preventing wet compression in a heat pump.

1.2. Contribution, research gap and previous work

In the area of heat pump design, holistic optimization is a growing research field. If complex analysis is involved, mostly single components are integrated in the design process and there is rarely a detailed focus on the architecture of the optimization itself. There is a lot potential, to investigate the optimization architecture to be independent from integrated tools and heat pump type. This is a key research objective of the present work, which aims to minimize function evaluations to make holistic concepts more accessible to integrate complex models to produce reliable results. This paper presents generalizable concepts for holistic heat pump optimization that integrate multiple detailed component analyses. The proposed concept is applicable to any heat pump problem and provides a pathway for improved decision-making in the design process. In earlier work by Gollasch et al., the optimizations of the compressor and heat exchangers were integrated with the cycle optimization of a closed Brayton-cycle heat pump, resulting in an optimization problem with up to 75 parameters [27,28]. Two optimization approaches were compared starting with an AAO architecture and decoupling the heat exchanger optimization in a second structure. In conclusion, the decoupled approach has been found to be suitable for single- and multi-objective optimization and is superior to AAO. The distribution of the component optimization has proven to be beneficial for stability and convergence rate. This work is extended in [29,30], with the investigation of a distributed CO structure focusing on the comparison of regression methods to approximate the component analyses. Convergence for single- and multi-objective optimization is improved in relation to the initial studies.

1.3. Outline and research questions

This paper focuses on the comparative investigation of holistic optimization concepts. It builds on previous work and altogether 4 different optimization architectures for a reversed Brayton heat pump are analyzed. First, the underlying methods for modeling and the optimization structures are introduced. A feature sensitivity and error propagation study is performed showing the impact of component efficiencies on cycle performance. This is followed by discussing the

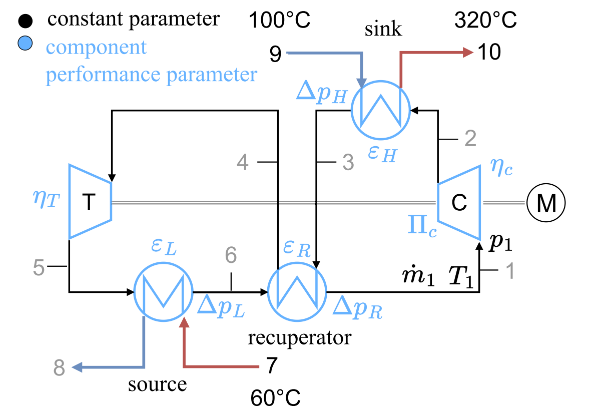

Fig. 1. Layout of a reversed Brayton cycle heat pump with recuperation. Cycle station values are optimized to reach the required heat sink energy with minimum drive power. In holistic structures, component performance parameters in blue are determined by integrated analyses.

training of surrogate models, which are analyzed concerning their prediction accuracy. In the results section, the optimization concepts are compared with consideration of required function evaluations, objective function values and parameter similarity. The following research questions are addressed:

1. To what extent does the performance of individual components influence the overall efficiency of the heat pump?
2. To what extent does uncertainty about component performances propagate through the process of cycle optimization?
3. Which architectures for multi-disciplinary optimization are best suitable for closed cycle heat pumps?
4. What is the impact of distributed cycle optimization within a collaborative optimization concept with regard to convergence, stability and numerical efficiency?
5. Do local surrogate models reach sufficiently low approximation errors while reducing overall function evaluations?
6. How can structures be generalized to more cycles while mitigating the risk of local approximation errors?

2. Modeling: Disciplinary analyses for heat pump design

Fig. 1 shows the layout of a reversed Brayton cycle heat pump. This air cycle heat pump is based on the inverted gas turbine cycle. It mainly consists of compressor, turbine and heat exchangers (HEX) for heat source and heat sink. Additionally, a recuperator is applied to transfer heat to the compressor inlet preventing high pressure ratios, which are usually unfavorable for the COP. A detailed analysis of this cycle was performed in [31]. A more in-depths introduction of the basic working principle can be found in [28]. In the present work, a mass flow of 32 kg/s of dry air is heated up from 100°C to 320°C (9 → 10). A mass flow of 35 kg/s and 60°C is available as heat source. These are the fixed boundary conditions for the holistic heat pump design studies performed in this work (also see Appendix A). The process requirements were chosen to roughly match a reference compressor design, whose geometry is adapted in the holistic optimization process. All heat pump state points (1–6) are determined during the optimization procedure and depend on the matching of most suitable component designs. In this work, 4 components are designed simultaneously with the cycle: A multi-stage axial compressor and the 3 heat exchangers. Only the turbine design is not integrated and treated with a constant efficiency. First studies by Gollasch et al. focused on the integration of compressor design, as it is the core component of all heat pump cycles. Furthermore, no suitable method for aerodynamic performance prediction of turbines was available to the authors at the time. For reasons of comparability with previous work, turbine integration is omitted in this paper. The integration of turbine models is further elaborated in Section 6.5. In Sections 2.1 to 2.3, the disciplinary analyses are introduced. For each discipline, the variable and constant input parameters as well as functional outputs are described. The integrated analyses are well-established methods that have been validated in the referenced literature.

2.1. Cycle analysis and integration in holistic design

Cycle analysis is based on 0D steady-state modeling. In this work, the performance simulations are performed with TesPy (Thermal Engineering Systems in Python) as introduced in [32]. With a suitable parameterization of the problem, an equation system is set up with variable parameters and constant boundary conditions. The state variables at each stations are determined with a Newton–Raphson algorithm.

$$\boldsymbol{y}_{\text{cyc}} = f(\boldsymbol{p}_{\text{cyc}}, \boldsymbol{x}, \boldsymbol{c}_{\text{cyc}}) \tag{1}$$

$$\boldsymbol{p}_{\text{cyc}} = [\eta_C, \eta_T, T_1, \Pi_c, \dot{m}_1, ttd_{\text{L}}, \boldsymbol{\Delta P}_j] \in \mathbb{R}^9$$

$$\text{with} \quad j \in \{\text{H, R, L}\}$$

$$\boldsymbol{c}_{\text{cyc}} = [T_7, \dot{m}_7, P_1, T_9, \dot{m}_9, T_{10}]$$

$$\boldsymbol{y} = [COP, \dot{Q}_H, \dot{Q}_L, \dot{Q}_R] \tag{2}$$

$$\boldsymbol{x} = (\boldsymbol{s}_i)_{i=1}^{n} \quad \text{with } \boldsymbol{s}_i = [T_i, \dot{m}_i, P_i]$$

The approach for the cycle analysis as it is embedded in the holistic optimization concepts is shown in Eq. (1). The efficiency parameters of the components need to be accessible to be set as variable parameters $\boldsymbol{p}_{\text{cyc}}$. This includes efficiency of compressor η_C and turbine η_T, pressure ratio Π_C and the HEX parameters ttd (terminal temperature difference) as well as pressure drops $\boldsymbol{\Delta P}_j$. Furthermore, the boundary conditions with the process demands for the heat pump are set as constant parameters $\boldsymbol{c}_{\text{cyc}}$. These are usually the conditions for the heat sink and the available inflow for the heat source. The system states $\boldsymbol{x}$ and the outputs $\boldsymbol{y}$ are computed. This includes the heat pumps coefficient of performance $COP = \dot{Q}_H / \dot{W}_C$ and heat flow rates $\dot{Q}_j$ with $j \in \{\text{H, L, R}\}$ for all heat exchangers, where H is the sink HEX, L the source HEX and R the recuperator. The exemplary parameterization needs to be adapted to match the holistic optimization architecture and its interfaces. In cycle design, values like the mass flow $\dot{m}_1$ and pressure ratio Π_C are optimized for the minimum driving power $\dot{W}_{el}$.

2.2. Aerodynamic compressor analysis

A generic framework is applied to design compressors from scratch based on assembling stages from reference geometries. The design process uses automated scaling for varying inflow conditions, which is why this procedure is tailored to find feasible designs for a wide range of design points. This is a requirement for the integration in holistic optimization. Additionally, the analysis needs to produce a smooth functional response with reliable predictions of the performance. Geometry generation and numerical setup are described in more detail in [28] and in the Appendix C. The compressor analysis is based on aerodynamic simulations with the in-house throughflow software ACDC (Advanced Compressor Design Code). ACDC features a 2D streamline curvature solver and a database of pre-optimized airfoils that are automatically allocated [33]. Flow turning and loss correlations are tuned based on this airfoil family and accurate predictions of pressure ratio, efficiency and stability are enabled [34].

$$\boldsymbol{y}_{\text{C}} = f(\boldsymbol{p}_C, \boldsymbol{c}_C, \boldsymbol{s}_1) \tag{3}$$

$$\boldsymbol{p}_C = [\boldsymbol{\pi}_r, \boldsymbol{\beta}_s, \omega, \boldsymbol{r}_i, \boldsymbol{\alpha}_h] \in \mathbb{R}^{35}$$

$$\boldsymbol{c}_C = [\boldsymbol{\alpha}_s, \boldsymbol{n}_b, \boldsymbol{l}_{ch.}]$$

$$\boldsymbol{y}_C = [\eta_C, \Pi_C, \boldsymbol{h}_C] \tag{4}$$

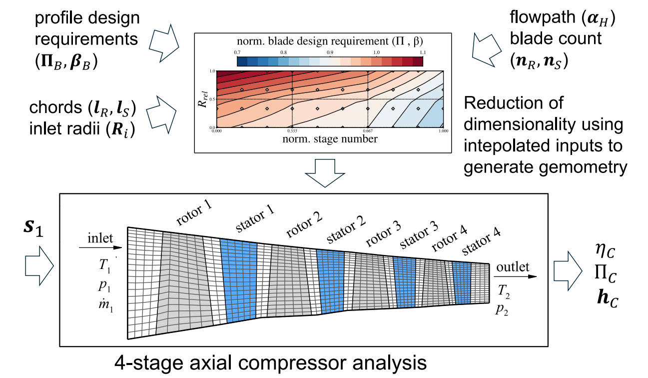

Fig. 2. Generic compressor design for variable inlet conditions using concepts for dimensionality reduction. The compressor can be designed from scratch using automated scaling.

$$\boldsymbol{h}_C = [\boldsymbol{c}_{\text{dif.}}, \boldsymbol{c}_{\text{flow}}, \boldsymbol{c}_{\text{Koch}}] \tag{5}$$

ACDC is integrated in the generic design framework, where a multi-stage compressor is generated for specified inflow conditions $\boldsymbol{s}_1 = [T_1, P_1, \dot{m}_1]$ (Fig. 2). The geometry is defined by setting radii, flowpath, blade positions and design requirements for the blades. Spline interpolation is used for parameter reduction to set the blade parameters independently from the number of stages. The splines contain parameters for blade design ($\boldsymbol{\Pi}_B$, $\boldsymbol{\beta}_B$), hub taper angle $\boldsymbol{\alpha}_H$, inlet radii $\boldsymbol{r}_i$ and rotational speed ω. For each compressor design, values for isentropic efficiency η_C and pressure ratio Π_C are computed. Together with the inflow conditions s_1 these are also the interface parameters to the cycle evaluation. Additionally, a vector of constraint functions $\boldsymbol{h}_c$ is returned that ensures feasible compressor designs. These inequality constraints consist of stability parameters such as flow coefficients, diffusion factor and the Koch criterion [35]. The design vector for a single compressor in Eq. (3) consists of 35 parameters. To reduce complexity, constant parameters $\boldsymbol{c}_C$ are used for the shroud taper angles, the blade count and chord lengths.

The effects of automated scaling are underlined in Fig. 3(a) where $N = 8000$ randomly generated compressor designs (latin hypercube sampling method - lhs) are evaluated:

$$\{(\Pi_c^{(i)}, \eta^{(i)})\}_{i=1}^{N=8e3} \quad \text{with} \quad \eta^{(i)}, \Pi_c^{(i)} = f(\boldsymbol{p}_c^{(i)}, \boldsymbol{s}_1^{(i)})$$

For the specified parameter bounds, the resulting pressure ratios range between 3.8 and 5.2. The black line highlights the trend of most efficient designs. Higher pressure ratios invoke a drop in efficiency, which is caused by aerodynamic loss mechanisms. For pressure ratios $\Pi_c \leq 4.2$ unfavorable designs are produced. Depending on the search space of holistic heat pump design, parameter bounds or number of stages might need to be adapted. The temperature requirements of the heat pump in this work are chosen to match this range of pressure ratios. Fig. 3 underlines that the best achievable compressor designs are independent from the inflow conditions of temperature T_1 and mass flow $\dot{m}_1$. The trend of the maximum efficiency is constant for the entire range, which is the effect of automated scaling. The generation of a single compressor design and evaluation of stability can take up to 60 s. The compressor in this work is based on the existing DLR-Rig250 [36]. The initial geometry is scaled and modified by the optimizer to match the requirements of the heat pump cycle. ACDC has been validated against CFD results [34] and experimental data [37].

2.3. Heat exchanger analysis: Heat transfer and pressure drop

The heat exchanger analysis is performed with an in-house tool for the rating of shell-and-tube heat exchangers. It is mainly based on the widely established methods for calculating heat flow rates and pressure

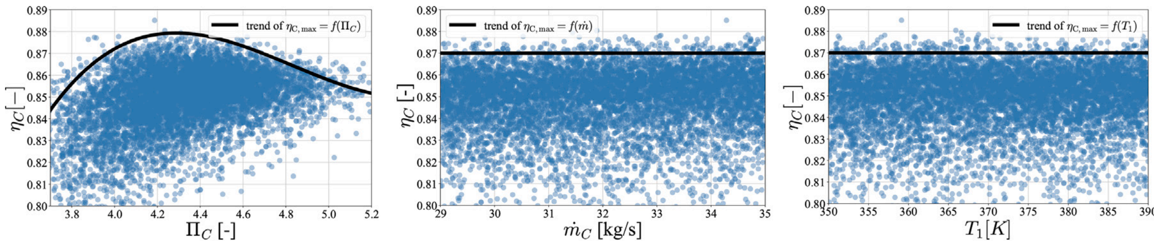

(a) (b) (c)

Fig. 3. Scattered data showing the trade-off between efficiency and pressure ratio (a) and the independence of compressor designs from inflow conditions as the consequence of automated scaling (b), (c)

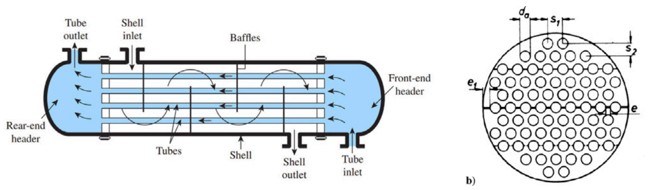

Fig. 4. Geometric parameters of shell and tube heat exchangers [38,40].

drop as described in [38]. Geometric parameters and inflow conditions are taken as inputs and heat transfer as well as pressure drop are computed. In this work, the heat flow rate $\dot{Q}$ is computed based on the P-NTU method, where P is the dimensionless temperature change and NTU is the number of transfer units. Tube side pressure drop ΔP_t is calculated with friction coefficients for turbulent and laminar flows based on their Reynolds numbers. Shell side pressure drop ΔP_s calculation is more complex and contains flow effects in cross flow and window zones of the tube bundles. The empirical correlations for heat transfer and pressure drop are provided in Appendix B. Additionally, functions from the library ChEDL (ht: Heat Transfer component of Chemical Engineering Design Library) are applied for the calculation of the shell diameter based on established design rules as well as using geometrical constraints to prevent vibrations [39].

Fig. 4 shows the geometry of shell and tube heat exchangers. The design parameters $\boldsymbol{p}_j$ used in this work are tube length l_t, tube diameter r_t, number of tubes n_t, tube spacing s_2 and baffle count n_B.

$$\boldsymbol{y}_j = f(\boldsymbol{p}_j, \boldsymbol{s}_{\text{in,hot}}, \boldsymbol{s}_{\text{in,cold}}) \tag{6}$$

$$\boldsymbol{p}_j = [d_t, l_t, n_t, s_2, n_{\text{B}}] \in \mathbb{R}^5$$

$$\boldsymbol{y}_j = [\dot{Q}_j, \Delta P_{\text{j, t}}, \Delta P_{\text{j, s}}, \boldsymbol{s}_{\text{j,t}}, \boldsymbol{s}_{\text{j,s}}] \tag{7}$$

with $j \in \{\text{H, L, R}\}$

For each heat exchanger $j \in \{\text{H, L, R}\}$, heat flow rate $\dot{Q}_j$, pressure drops $\boldsymbol{\Delta P}_j = [\Delta P_{t,j}, \Delta P_{s,j}]$ and the outflow states $\boldsymbol{s}_{\text{out},j}$ are returned from the analysis. For the recuperated Brayton cycle, three heat exchangers with an overall number of 15 design parameters are considered in this work. The inflow conditions on both sides are given as a boundary conditions. The analysis is of low computational cost and takes a fraction of a second. Nevertheless, as a preparation for future work the number of overall function evaluations is kept low to prepare the integration of more costly analyses.

3. Holistic optimization architectures

Each discipline brings an analysis with its design parameters into the holistic optimization problem. In closed cycles, all thermodynamic states are interactively affected by component performance, meaning that their design points are interdependent. The architecture of the optimization problem refers to the communication processes between the top-level optimizer and integrated disciplines to solve a holistic problem. Choice of interface parameters, splitting the design vectors to solve subproblems as well as selecting algorithms are part of the methodological framework.

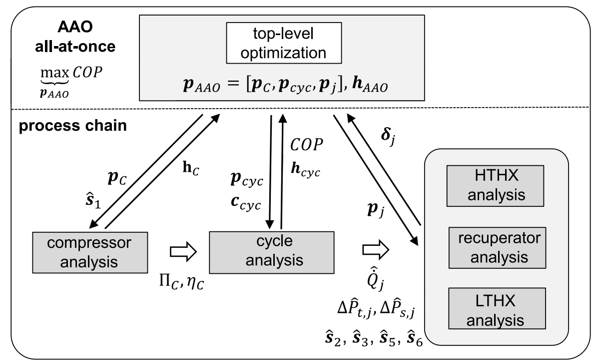

Fig. 5. All-at-once optimization structure: All design parameters $\boldsymbol{p}_{\text{AAO}}$ are handled by the top-level optimizer.

3.1. All-at-once optimization

Algorithm 1 All-at-once optimization.

Top-level: Initial DoE and training of Kriging surrogates for all objectives and constraints
while $COP[10] \leq COP[1] + 1\text{e}{-3}$ **do**
Set global $\boldsymbol{p}_{\text{AAO}} = [\boldsymbol{p}_{\text{C}}, \boldsymbol{p}_{\text{cyc}}, \boldsymbol{p}_{\text{j}}]$ with Bayesian optimization and genetic operators
Evaluate compressor design with $\boldsymbol{p}_{\text{C}} \subseteq \boldsymbol{p}_{\text{AAO}}$ and inflow conditions $\boldsymbol{s}_1 \subseteq \boldsymbol{p}_{\text{AAO}}$. Return $\boldsymbol{h}_C$ to top-level and pass $\boldsymbol{y}_C = [\eta_C, \Pi_C]$ to cycle evaluation.
Evaluate the thermodynamic cycle with $\boldsymbol{y}_C$ and $\boldsymbol{p}_{\text{cyc}} \subseteq \boldsymbol{p}_{\text{AAO}}$. Return the objective function value COP and $\boldsymbol{h}_{\text{cyc}}$. Pass design targets $[\hat{\dot{Q}}, \Delta\hat{P}_{t,j}, \Delta\hat{P}_{s,j}, \boldsymbol{s}_{\text{j,in}}]$ to HEX analysis.
Perform the HEX-analysis with $\boldsymbol{p}_j \subseteq \boldsymbol{p}_{\text{AAO}}$. Return deviation from the target values δ_j to top-level optimizer.
Update the Kriging surrogates for objectives and constraints.
end while

The first optimization architecture is all-at-once optimization (AAO). In this non-distributed structure, a single large optimization problem is formulated. As shown in Fig. 5, all design variables are handled by the top-level optimizer, which results in high dimension of the design vector. The pseudo-algorithm is formulated in Algorithm 1 and starts with the execution of the compressor analysis. Each compressor design (η_C, Π_C) is evaluated in the thermodynamic cycle analysis with the results of the aerodynamic modeling. Interfacing parameters are the inlet conditions $\boldsymbol{s}_1$, efficiency η_C as well as pressure ratio Π_C. As a last step, HEX designs are evaluated with parameters $\boldsymbol{p}_j$ also set by the top-level optimizer. As a consequence, these designs are not necessarily consistent with the targets of the cycle configuration in

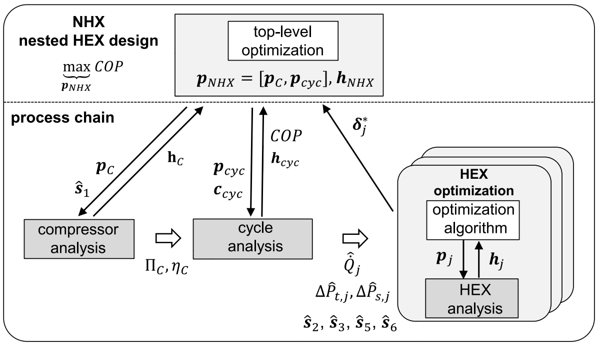

Fig. 6. Nested heat exchanger design optimization structure: Heat exchangers are optimized in subproblems for target values.

terms of heat transfer $\hat{\dot{Q}}_j$ and pressure drop $\Delta\hat{\boldsymbol{P}}_j$. To meet these targets, constraint functions $\boldsymbol{h}_j$ are introduced that restrict the feasible solutions to configurations where the HEX designs match the cycle simulation.

$$\max_{p_{AAO}\in} COP = \frac{\dot{Q}_H}{\dot{W}_{\text{in}}} \text{ s.t. } \boldsymbol{h}_{AAO} \leq \boldsymbol{\zeta}_{AAO} \tag{8}$$

$$\boldsymbol{p}_{AAO} = [\boldsymbol{p}_C, \boldsymbol{p}_{cyc}^{AAO}, \boldsymbol{p}_j] \in \mathbb{R}^{60} \tag{9}$$

$$\boldsymbol{p}_{\text{cyc}}^{\text{AAO}} = [\dot{m}, T_1, ttd_L, \Delta\boldsymbol{P}_{t,j}, \Delta P_{s,R}]$$

with $j \in \{\text{H, L, R}\}$

$$\boldsymbol{h}_{AAO} = [\boldsymbol{h}_C, \boldsymbol{h}_j = \|\boldsymbol{\delta}_j\|_2, \boldsymbol{h}_{\text{cyc}}] \tag{10}$$

$$\boldsymbol{h}_C = [\boldsymbol{c}_{\text{dif.}}, \boldsymbol{c}_{\text{flow}}, \boldsymbol{c}_{\text{Koch}}] \tag{11}$$

$$\boldsymbol{\delta}_j = [|\dot{Q}_j - \hat{\dot{Q}}_j|, |\Delta P_{t,j} - \Delta\hat{P}_{t,j}|, |\Delta P_{s,j} - \Delta\hat{P}_{s,j}|] \tag{12}$$

Eqs. (8)–(12) show the formulation of AAO. The approach is evaluated with direct integration of analyses in [28]. Overall 60 design variables are optimized, while 35 define the complex compressor design.

$$\boldsymbol{\delta}_j(\boldsymbol{p}_j) = \begin{cases} (\boldsymbol{y}_j - \hat{\boldsymbol{y}}_j) & \text{if } |\boldsymbol{y}_j - \hat{\boldsymbol{y}}_j| > \zeta j \\ 0 & \text{otherwise} \end{cases} \tag{13}$$

$$\text{with } \quad \boldsymbol{y}_j = [\dot{Q}_j, \Delta P_{\text{t,j}}, \Delta P_{\text{s,j}}] \tag{14}$$

The constraint functions are the deviations $\boldsymbol{\delta}_j$ between cycle target and HEX analysis and need to reach a tolerable threshold $\boldsymbol{\zeta}_j$. For AAO, there are deviation terms for the heat flow rate $|\dot{Q}_j - \hat{\dot{Q}}_j|$ and pressure drops $|\Delta\boldsymbol{P}_j - \Delta\hat{\boldsymbol{P}}_j|$, as formulated in Eq. (14). The AAO architecture is characterized by a fast evaluation of the process chain but low convergence rate. This is expected, as the constraints for matching HEX designs need to be controlled first. This is highly dependent on the initial database and it can take a high number of top-level evaluations until a feasible solution is found that can be improved by the optimizer. This concept will be considered in the discussions but apart from that not further analyzed in this work.

3.2. Nested heat exchanger design

In order to overcome the shortcomings of AAO, nested-heat-exchanger-design (NHX) is introduced as a second optimization structure. Here, the heat exchanger optimization is solved as a distributed subproblem. The concept is based on reducing the top level problem and avoid infeasible HEX. The heat exchanger optimization is now performed for target requirements $\hat{\dot{Q}}, \hat{\boldsymbol{P}}_j$ that are calculated by the cycle evaluation (Fig. 6). If feasible HEX are found, the designs are already matched to the cycle states. The feasibility is controlled with the deviation terms $\boldsymbol{\delta}_j$ that are returned to the top-level optimizer. This subproblem optimization needs to be repeated for each top-level iteration and therefore requires a fast analysis (Algorithm 2). In this work, the HEX analysis is a Python script and the optimization can be performed in less than 5 min. wallclock time.

Algorithm 2 NHX.

Top-level: Initial DoE and training of Kriging surrogates for all objectives and constraints
1: **while** $COP[10] \leq COP[1] + 1\text{e}{-3}$ **do**
2: Set global $\boldsymbol{p}_{\text{NHX}} = [\boldsymbol{p}_{\text{C}}, \boldsymbol{p}_{\text{cyc}}]$ with Bayesian optimization and genetic operators
3: Evaluate compressor design with $\boldsymbol{p}_{\text{C}} \subseteq \boldsymbol{p}_{\text{NHX}}$ and inflow conditions $\boldsymbol{s}_1 \subseteq \boldsymbol{p}_{\text{NHX}}$. Return $\boldsymbol{h}_C$ to top-level and pass $\boldsymbol{y}_C = [\eta_C, \Pi_C]$ to cycle evaluation.
4: Evaluate the thermodynamic cycle with $\boldsymbol{y}_C$ and $\boldsymbol{p}_{\text{cyc}} \subseteq \boldsymbol{p}_{\text{NHX}}$. Return the objective function value COP and $\boldsymbol{h}_{\text{cyc}}$. Pass design targets $[\hat{\dot{Q}}, \Delta\hat{P}_{t,j}, \Delta\hat{P}_{s,j}, \boldsymbol{s}_{\text{j,in}}]$ to HEX analysis.
5: Perform the HEX-optimization for target values with local $\boldsymbol{p}_j \not\subseteq \boldsymbol{p}_{\text{NHX}}$. Trace if feasible designs are found by returning minimized deviations δ_j^*.
6: Update the Kriging surrogates for objectives and constraints.
7: **end while**

top-level optimization:

$$\max_{p_{NHX}} COP = \frac{\dot{Q}_H}{\dot{W}_{\text{in}}} \text{ s.t. } \boldsymbol{h}_{NHX} \leq \boldsymbol{\zeta}_{NHX} \tag{15}$$

$$\boldsymbol{p}_{NHX} = [\boldsymbol{p}_C, \boldsymbol{p}_{cyc}^{NHX}] \in \mathbb{R}^{45} \tag{16}$$

$$\boldsymbol{p}_{\text{cyc}}^{\text{NHX}} = [\dot{m}, T_1, \hat{ttd}_L, \Delta\hat{\boldsymbol{P}}_{t,j}, \Delta\hat{P}_{s,R}]$$

$$\boldsymbol{h}_{NHX} = [\boldsymbol{h}_C, \boldsymbol{h}_j = \|\boldsymbol{\delta}_j^*\|_2, \boldsymbol{h}_{\text{cyc}}] \tag{17}$$

$$\boldsymbol{h}_C = [\boldsymbol{c}_{\text{dif.}}, \boldsymbol{c}_{\text{flow}}, \boldsymbol{c}_{\text{Koch}}] \tag{18}$$

subproblem optimization:

heat exchanger optimization

$$\min_{p_j \in \mathbb{R}^5} \; l_j + \lambda_j^\top \, \boldsymbol{\delta}_j^2, \; j \in \{\text{H, L, R}\} \tag{19}$$

$$\boldsymbol{\delta}_j = [|\dot{Q}_j^* - \hat{\dot{Q}}_j|, |\Delta P_{t,j}^* - \Delta\hat{P}_{t,j}|, |\Delta P_{s,j}^* - \Delta\hat{P}_{s,j}|] \tag{20}$$

The optimization problem is formulated in (15)–(19). On top-level, the dimensions are reduced and the optimizer now handles only the compressor and cycle parameters. The constraint functions contain the euclidean norm of the deviation vectors $\boldsymbol{h}_j = \|\boldsymbol{\delta}_j^*\|_2$ returned from HEX design. For HEX optimization, a single-objective optimization problem is solved minimizing the heat exchanger length l_j while deviations from targets are penalized in form of quadratic penalty terms $\lambda_j^\top \, \boldsymbol{\delta}_j^2$. Here, λ is a weight function for the constrained design targets. Similar to AAO, the deviations are activated above relaxation thresholds as introduced in Eq. (14). Previous work has shown, that reliability and convergence rate are significantly improved with this approach. Feasible designs are detected earlier and objective functions values are better compared to AAO.

3.3. Collaborative design

To follow this path, collaborative design (CD) is introduced as a fully distributed optimization structure. All components are optimized in subproblems for target values derived from the thermodynamic cycle analysis.

Fig. 7 shows the structure of collaborative optimization. In a first step, the cycle is evaluated by setting all component target parameters in $\boldsymbol{p}_{\text{cyc}}^{\text{CD}}$. All system states are simulated and used as inputs for component optimizations. The subproblems are executed to find feasible compressor and HEX designs. The process is described in Algorithm 3. Compressor optimization is performed with local parameters $\boldsymbol{p}_C \not\subseteq \boldsymbol{p}_{\text{CD}}$.

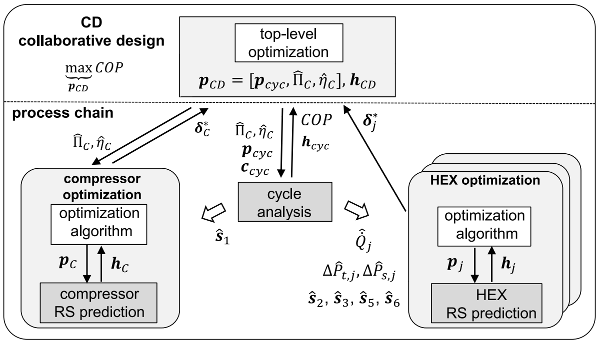

Fig. 7. Collaborative design optimization structure: The cycle is evaluated in a first step. Compressor and heat exchanger optimization is performed for target values in subproblems.

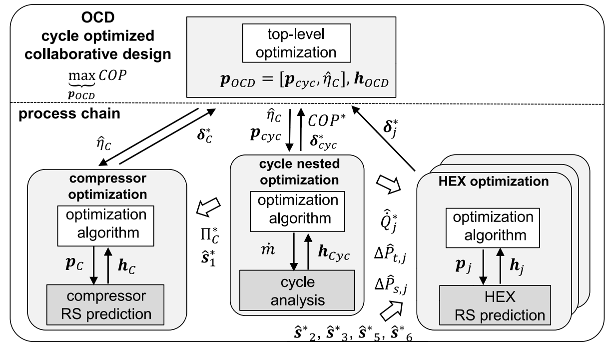

Fig. 8. Cycle optimized collaborative design optimization structure: The cycle is optimized in a subproblem. Compressor and heat exchanger optimization is performed for target values and optimal cycle states.

Algorithm 3 CD.

Top-level: Initial DoE and training of Kriging surrogates for all objectives and constraints

1: **while** $COP[10] \leq COP[1] + 1\text{e}{-3}$ **do**
2: Set global p_{CD} containing target values with Bayesian optimization and genetic operators
3: Evaluate the thermodynamic cycle with target component efficiency parameters and mass flow rate. Return the objective function value COP and h_{cyc}. Pass the design targets and station values to compressor and HEX analysis: $[s_1, \hat{\eta}_C, \hat{\Pi}_C]$, $[\hat{Q}, \Delta\hat{P}_{t,j}, \Delta\hat{P}_{s,j}, s_{\text{j,in}}]$.
4: Perform subproblem optimization with local $p_C \not\subseteq p_{\text{CD}}$ to find feasible compressors. Return minimized deviation from targets δ_C^*.
5: Perform local target optimization with local $p_j \not\subseteq p_{\text{CD}}$ to find feasible HEX. Return minimized deviation from targets δ_j^*.
6: Update the Kriging surrogates for objectives and constraints.
7: **end while**

Minimized deviations from targets δ_C^* are returned to the top-level. The heat exchanger subproblem optimization is identical to NHX.

top-level optimization:

$$\max_{p_{CD}} COP = \frac{\dot{Q}_H}{\dot{W}_{\text{in}}} \text{ s.t. } h_{CD} \leq \zeta_{CD} \tag{21}$$

$$p_{\text{CD}} = [\hat{\eta}_C, \hat{\Pi}_C, p_{\text{cyc}}^{\text{CD}}] \in \mathbb{R}^9$$

$$p_{\text{cyc}}^{\text{CD}} = [\hat{ttd}_j, \Delta\hat{P}_{t,j}, \Delta\hat{P}_{s,R}]$$

with $j \in \{\text{H, L, R}\}$

$$h_{\text{CD}} = [\|\delta_C^*\|_2, \|\delta_H^*\|_2, \|\delta_R^*\|_2, \|\delta_L^*\|_2] \tag{22}$$

subproblem optimization:

heat exchanger optimization

$$\min_{p_j \in \mathbb{R}^5} l_j + \lambda_j^{\top} \delta_j^2, \; j \in \{\text{H, L, R}\} \tag{23}$$

$$\delta_j = [|\dot{Q}_j^* - \hat{\dot{Q}}_j|, |\Delta P_{t,j}^* - \Delta\hat{P}_{t,j}|, |\Delta P_{s,j}^* - \Delta\hat{P}_{s,j}|] \tag{24}$$

compressor optimization

$$\min_{p_c \in \mathbb{R}^{35}} |\eta_c - \hat{\eta}_c| + \lambda_C^{\top} \delta_C^2 \tag{25}$$

$$\delta_C = [\Pi_C - \hat{\Pi}_C, \delta_{\{h_C \leq \zeta_C\}}] \tag{26}$$

The optimization problem is formulated in Eqs. (21)–(26). The top-level optimizer sets the target values with p_{CD}, which drastically reduces the dimensions of the problem to 8 parameters. Additionally, the stability constraints of the compressor are also distributed to the compressor subproblem optimization. All subproblems are formulated as single objective optimizations treating the constraints as penalty terms so that the magnitude of deviations is traceable. On top level, vector norms of δ_C are kept below relaxation thresholds ζ_C to account the compressor design as feasible for the defined performance targets. This compressor subproblem is computationally expensive if performed directly with detailed throughflow analysis (Section 2.2). A single target optimization as a subproblem can take up to several hours, which is not suitable for integration in distributed holistic concepts to avoid extensive computation time. For this reason, the optimization is performed with computationally inexpensive surrogate models in the present work. The formulation of the subproblem is shown in Eq. (25). Deviations from the target efficiency $|\eta_C - \hat{\eta}_C|$ are minimized as the objective function. Pressure ratio targets $\hat{\Pi}_C$ are considered as relaxed equality constraints and treated by using quadratic penalty terms that are activated if violation occurs. This represents a transformation to inequality constraints and the penalties are switched off if a threshold is reached, as described in Eq. (14).

$$\delta_2(p) = \begin{cases} (c_{\text{Koch}} - \hat{c}_{\text{Koch}}) & \text{if } c_{\text{Koch}} > \zeta_{c,2} \\ 0 & \text{otherwise} \end{cases} \tag{27}$$

This is done in a similar way for the remaining c_{diff} and c_{Koch} inequality constraints for stability coefficients in Eq. (27). These penalties are only activated if threshold accuracy is not reached. In this way, the top-level optimizer gets a feedback δ_C if the design requirements invoke infeasible compressor designs. The distributed nature of this optimization approach drastically reduces top-level complexity. It is initially investigated with focus on different regression methods in [29,30].

3.4. Cycle optimized collaborative design

Algorithm 4 OCD.

Top-level: Initial DoE and training of Kriging surrogates for all objectives and constraints

1: **while** $COP[10] \leq COP[1] + 1\text{e}{-3}$ **do**
2: Set global p_{OCD} containing target values with Bayesian optimization and genetic operators
3: Optimize the thermodynamic cycle with target component efficiency parameters. Return the objective function value COP^* and h_{cyc}. Pass the design targets and station values to compressor and HEX analysis: $[s_1^*, \hat{\eta}_C, \hat{\Pi}_C]$, $[\hat{Q}^*, \Delta\hat{P}_{t,j}, \Delta\hat{P}_{s,j}, s_{\text{j,in}}^*]$.
4: Perform the subproblem optimization with local $p_C \not\subseteq p_{\text{OCD}}$ to find feasible compressors. Return minimized deviation from targets δ_C^*.
5: Perform target optimization with local $p_j \not\subseteq p_{\text{OCD}}$ to find feasible HEX. Return minimized deviation from targets δ_j^*.
6: Update the Kriging surrogates for objectives and constraints.
7: **end while**

Cycle-optimized collaborative design is introduced as an upgrade to CD. Here, the cycle optimization is solved as a subproblem. Fig. 8

and Algorithm 4 show the structure of OCD. In a first step, the cycle is optimized for the target efficiency values of the components as defined by the top-level parameters $\boldsymbol{p}_{\text{OCD}}$. As a consequence, the component target optimizations are always performed for optimal cycle system states as these are passed as design points. The top-level optimizer orchestrates the deviations $\boldsymbol{\delta}$ as constraints to find limits of feasible component targets that are usually near their maximum performance capability.

top-level optimization:

$$\max_{\boldsymbol{p}_{\text{OCD}}} COP = \frac{\dot{Q}_H}{\dot{W}_{\text{in}}} \text{ s.t. } \boldsymbol{h}_{OCD} \leq \boldsymbol{\zeta}_{OCD} \tag{28}$$

$$\boldsymbol{p}_{\text{OCD}} = [\hat{\eta}_C, \boldsymbol{p}_{\text{cyc}}^{\text{OCD}}] \in \mathbb{R}^8 \tag{29}$$
$$\boldsymbol{p}_{\text{cyc}}^{\text{OCD}} = [\hat{ttd}_j, \Delta\hat{\boldsymbol{P}}_{t,j}, \Delta\hat{P}_{s,R}]$$
with $j \in \{\text{H, L, R}\}$

$$\boldsymbol{h}_{\text{OCD}} = [\|\boldsymbol{\delta}_C^*\|_2, \|\boldsymbol{\delta}_H^*\|_2, \|\boldsymbol{\delta}_R^*\|_2, \|\boldsymbol{\delta}_L^*\|_2] \tag{30}$$

subproblem optimization:

cycle optimization

$$\max_{[\dot{m}]} COP \tag{31}$$

$$\boldsymbol{c}_{\text{cyc}}^{\text{cyc}} = \boldsymbol{p}_{\text{cyc}}^{\text{OCD}} \subseteq \boldsymbol{p}_{\text{OCD}} \tag{32}$$

heat exchanger optimization

$$\min_{\boldsymbol{p}_j \in \mathbb{R}^5} l_j + \boldsymbol{\lambda}_j^{\top} \boldsymbol{\delta}_j^2, \; j \in \{\text{H, L, R}\} \tag{33}$$

$$\boldsymbol{\delta}_j = [|\dot{Q}_j^* - \hat{\dot{Q}}_j|, |\Delta P_{t,j}^* - \Delta\hat{P}_{t,j}|, |\Delta P_{s,j}^* - \Delta\hat{P}_{s,j}|] \tag{34}$$

compressor optimization

$$\min_{\boldsymbol{p}_c \in \mathbb{R}^{35}} |\eta_c - \hat{\eta}_c| + \boldsymbol{\lambda}_C^{\top} \boldsymbol{\delta}_C^2 \tag{35}$$

$$\boldsymbol{\delta}_C = [\Pi_C - \hat{\Pi}_C, \boldsymbol{\delta}_{\{h_C \leq \zeta_C\}}] \tag{36}$$

The optimization problem is formulated starting with Eq. (28). In comparison to CD, the cycle parameters $\boldsymbol{p}_{\text{cyc}}^{\text{OCD}}$ changed, as the mass flow rate $\dot{m}$ is a distributed parameter for the cycle optimization. Optimized results are mass flow $\dot{m}^*$ and pressure ratio Π_C^* that are now always perfectly matched with the process requirements. The top-level optimizer solely has the task to find the best combination of components, which is the true nature of holistic heat pump design.

3.5. Optimization algorithms

Efficient optimization algorithms are required to solve complex problems of multi-disciplinary design strategies. For this reason, the DLR in-house suite AutoOpti is applied for the top-level optimizations. AutoOpti features metamodel assisted global optimization and has proven to be efficient for complex tasks like turbomachinery design [41]. For each optimization run, an initial database is generated e.g. by using a latin hypercube approach. Metamodels based on Kriging regression are generated for all terms in the objective and constraint functions. To create new candidates, several methods can be applied. If the updated candidate is generated by searching on the metamodels, acquisitions functions for Bayesian optimization like expected improvement are evaluated based on the predictions. Additionally, genetic operators like differential evolution or mutation can be used to create new individuals. The chosen methods can be freely combined by setting weights for their application. After each evaluation of the process chain, the surrogate models are updated and promising candidates are stored in the database. This process is repeated until convergence is reached. For all inner component (subproblem) optimizations, differential evolution as implemented in the SciPy library is used [42,43]. Differential evolution is a well known method for black box optimization and applicable to a wide range of problems. As a downside, the algorithm may require a large number of function evaluations. In this work, the global search is limited to a specified number of generations and followed by a local refinement using gradient based SLSQP. The proposed concepts are applicable for both single- and multi-objective optimizations. Surrogate assisted optimization algorithms on top-level support good convergence and global exploration. This works best with a smooth functional response from the subproblems, which was considered in the proposed optimization concepts and the interaction between top- and subproblem level. There are many conceivable alternative combinations of algorithms for solving holistic design problems, whereby this investigation is not part of the present work.

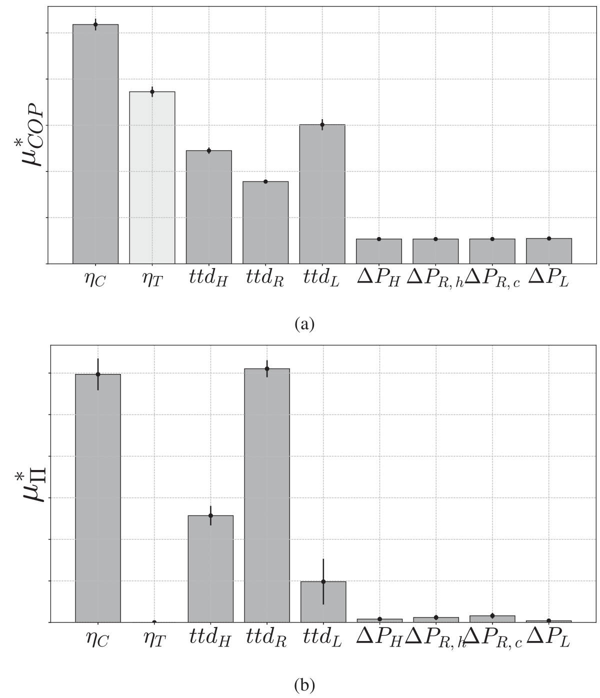

Fig. 9. Global sensitivity analysis of component parameters affecting (a) the optimized cycle COP^* and (b) the optimized pressure ratio Π^*, performed with the method by [44]. Overall parameter sensitivity: μ^*. The error bar is the standard deviation σ indicating the presence of interactions.

4. Sensitivity studies and propagation of uncertainty

Holistic design strategies with integrated component analyses reduce uncertainty by calculating the performance based on physical modeling and geometric sizing. To address the research questions 1 and 2 in Section 1.3, a global sensitivity study is performed followed by propagation of uncertainty about target efficiencies. Fig. 9 shows the results of the sensitivity study performed with the method by Morris [44–46]. Compressor efficiency η_C, turbine efficiency η_T and terminal temperature differences of the heat exchangers ttd_j are varied together with the pressure drops ΔP_j. These inputs represent the component designs that are integrated in holistic cycle optimization. For each set of inputs, the cycle is optimized for the maximum COP. The parameter μ^* in Fig. 9(a) represents the feature importance. All components have a significant impact on the COP. Within the analyzed parameter bounds, the compressor efficiency shows the highest sensitivity. For the HEX, the impact of heat transfer is dominant compared to the pressure drop. The turbine shows second highest impact but is not integrated in this study for the reasons discussed in Section 2. Fig. 9(b) additionally shows the sensitivity of the optimized pressure ratio Π. The compressor and recuperator show a high impact compared to the remaining HEX, which all interact, as indicated by the variance (error bars). The turbine has no impact, as its efficiency only affects

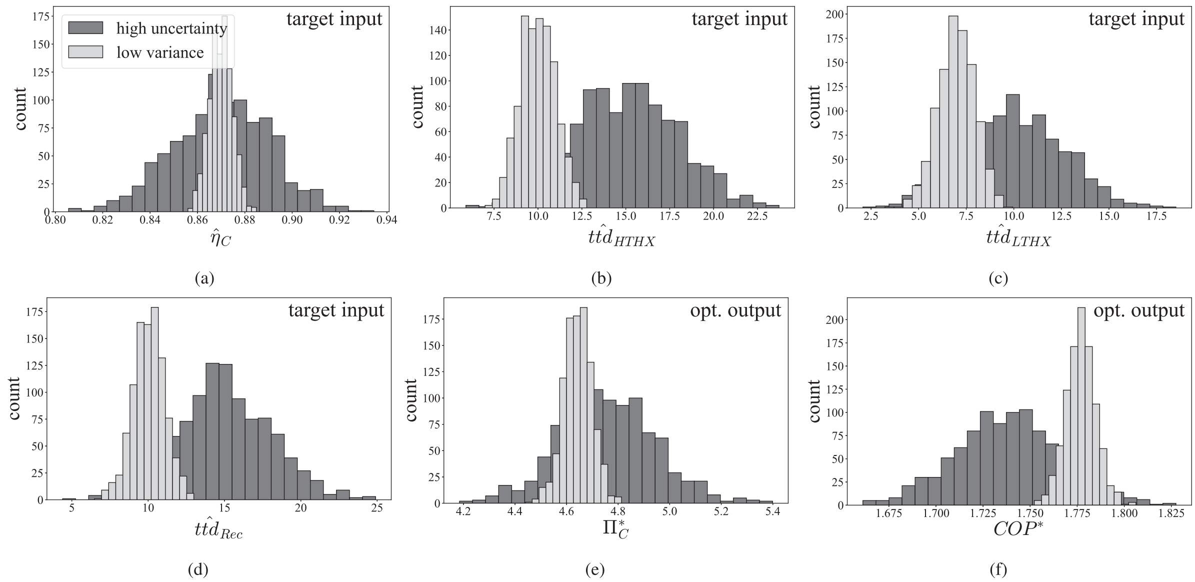

Fig. 10. Propagation of uncertainty about the component target performance. Input parameters are sampled from normal distributions ($p_i \sim \mathcal{N}(\mu, \sigma^2)$). Low variance: gray. High uncertainty: dark gray. The combined effects of target inputs (a–d) on the resulting distribution of optimized pressure ratio Π^* (e) and COP^* (f) are shown.

Table 1
Input distributions for uncertainty propagation.

Uncertainty	high		low	
Probability distribution	μ	σ	μ	σ
η_c	0.87	0.02	0.87	5e−3
ttd_H	15 K	3 K	10 K	1 K
ttd_R	15 K	3 K	10 K	1 K
ttd_L	10 K	3 K	7 K	1 K

turbine work and outlet temperature. This study indicates that precise knowledge of the performance of each component is crucial for cycle design.

Fig. 10 shows the combined effect of uncertainty about component performance on the optimized results as well as the direction of their impact. For this study, performance input parameters are sampled from Gaussian distributions. For each component, two sets of inputs with low and high variances are sampled. The large variance represents an indicator for high uncertainty as it would appear in sequential optimization approaches with independent cycle design. Fig. 10(a) – Fig. 10(d) highlight the frequency distribution of overall 1000 input samples for each component. For the HEX, the ttd values are shifted to smaller means to demonstrate their combined effect on result parameter distributions. All values used to define the normal distributions are summarized in Table 1. The effect on the optimized pressure ratios Π^* of the cycle is visualized in Fig. 10(e). The mean of Π^* is shifted to lower values with the improved HEX performance (light gray bars). This means, that the design point of the compressor is also impacted, which emphasizes the interaction with HEX design. The optimized COP^* shows a flat distribution with high variance in Fig. 10(f), which indicates the potential for errors caused by inaccurate assumptions. Improved HEX performances with lower ttd_j shift the mean of the COP to higher values.

In summary it can be stated, that heat pump efficiency is very dependent on its component designs, which are also highly interactive. These characteristics make the optimization problem more challenging, as components are required to be perfectly matched to reach the best cycle performance. Their interactions additionally lead to complications: As an example, compressor efficiency tends to decrease with higher pressure ratios. In conclusion, the cycle should not be designed independent of the components. Holistic design strategies can overcome these shortcomings if the component performances are accurately predicted.

5. Surrogate model training and validation

Subproblem optimizations in distributed structures invoke a high number of function evaluations for the component analyses, as described above. Using computationally inexpensive regression models to approximate their functional output enables to solve distributed problems in a reasonable time. In this work, surrogate models are trained to replace compressor and HEX analyses. Sampling strategies to minimize the training effort and global model accuracy are discussed. A low number of samples is important to demonstrate that the proposed holistic design concepts are also applicable when high dimensional simulations like CFD are integrated and function evaluations of the analysis become more costly.

Gaussian process regression (GPR) is capable to predict complex non-linear functions with a moderate amount of training data [47,48]. This agrees with the results of previous work by Gollasch et al. [29] showing that GPR is the most accurate method compared to linear regression and radial basis functions for both compressor and HEX approximation. For this reason, GPR models are used to investigate the optimization architectures in the present paper. GPR treats the functional output as a Gaussian distribution, yielding a predictive mean and variance: $f(\boldsymbol{p}) = \mathcal{N}\left(\mu(\boldsymbol{p}), \sigma^2(\boldsymbol{p})\right)$ [49]. The variance indicates the prediction error of the model and is essential for Bayesian optimization or for active learning. Static (single-step) and adaptive training strategies are considered to minimize the amount of required function evaluations for surrogate training in this work. For all models, the `GaussianProcessRegressor` class of scikit-learn [50] is applied. The radial basis function (RBF) kernel is used with vector length scales for each dimension. Training data is scaled (min–max scaler) and the kernel parameters are optimized during the fitting process.

5.1. Sampling strategies

The sampling strategy is crucial to train accurate surrogate models. Samples are aimed to be spread evenly throughout the design space with efficient space filling. As the dimensionality increases, a very high number of samples may be required for high global accuracy. In methods for design of experiments (DoE), there are several approaches to distribute samples across the search space. An even distribution on a regular grid as in full factorial design is directly dependent on the number of design variables. For this reason, factorial design is not suitable as it scales exponentially with the dimensions [51]. A fully random distribution of samples on the contrary is inefficient, as sufficient space filling can only be achieved with a high training effort [52]. Algorithms like latin hypercube sampling (LHS) allow to set the sample size independent from the size of the parameter vector [53]. It is therefore a flexible approach to randomly sample data while spreading sampled points evenly in the design space [54,55]. In this work, LHS is used for single stage sampling, which means that all sample points are generated in a single step.

Another key aspect of surrogate model training is information about the estimated local error of the surrogate. With this information available, two active learning concepts are considered in this work: Adaptive global surrogate training and contour estimation for local refinement.

5.2. Active learning strategies: Global and local exploration

DoE methods like latin hypercube sampling are based on providing space filling but do not guarantee a globally accurate surrogate model. Active learning strategies based on adaptive sampling strategically add samples in unexplored areas.

Algorithm 5 Active learning with global adaptive refinement.

```
Train initial model with n random samples
while σ̂_max(p) ≤ σ_max(p) do
1: optimize for max_p σ on GPR model
2: p* = arg max σ(p)
3: Evaluate function at: y = f(p*)
4: Append sample to training data
4: Train GPR with updated database
end while
```

Algorithm 5 shows the active learning strategy used to train a global surrogate based on adaptive refinement. The initial GPR model is generated with a low number of sample points generated with LHS. Now, the iterative procedure to refine the model starts: The position of the maximum local variance $\sigma(\boldsymbol{p})$ is detected by using optimization. This is the location with the highest assumed prediction error. Differential evolution is used to determine the parameter vector of the maximum standard deviation: $\boldsymbol{p}^* = \arg\max f(\boldsymbol{p})$. This vector can be interpreted as the location of the design space, which is least explored. The function output $f(\boldsymbol{p})$ of the analysis is appended to the training data set and the GPR model is updated. This procedure is repeated until a convergence criterion like a tolerable maximum variance is reached. As a downside, the repetitive training of the GPR models can create a bottleneck for larger databases, as the training effort scales in the order of $\mathcal{O}(n^3)$ for n samples. There are further global infill strategies like sequential LHS as discussed in [29]. This method applies epochal multi-sample updated but requires hyperparameter tuning and is not considered in this paper.

In some cases, high global model accuracy may not be required as only certain regions of the function are of interest. Local models that are only refined near target values may decrease training effort. The remaining space remains unexplored. First, local sub-spaces need to be identified, where the function is supposed to be approximated with highest accuracy. There are several ways to train local models using GPR. Contour estimation uses an acquisition function based on the expected improvement (EI) criterion [56]. It is formulated with the goal to identify sample positions that have the highest probability to improve the model near the target contour with a limited amount of global exploration [57]. The algorithm for contour estimation is equivalent to global active learning with one exception: The next sample is determined with the EI criterion: $\boldsymbol{p}^* = \arg\max E(I(\boldsymbol{p}))$. Optimization of this function will provide the next sample location $\boldsymbol{p}^*$ to improve the model near the contour value. This can also be extended for a wider region of interest by using multiple contour lines [58]. As a further note, contour estimation is a promising candidate for distributed holistic optimization strategies with online adapted surrogate models. This means the surrogates are refined in regions where the top-level optimizer is guiding target values for component design. Local updates can potentially be refined by adding multiple samples near contour lines.

Fig. 11 shows an exemplary two dimensional adaptive training of a GPR model with the heat exchanger analysis. The heat flow rate $\dot{Q}$ is predicted based on the parameters tube length l_t and number of tubes n_t. A global model is trained with adaptive refinement in Fig. 11(a). The red points are initial LHS samples, which are clearly randomly distributed. Active learning is then placing new samples until convergence is achieved (Fig. 11(b)). As a downside of this approach, the borders are explored first as the highest variances usually occur there. Only after that, the inner space is filled with evenly distributed points keeping some distance to the initial samples. Fig. 11(c) shows sampling with the contour estimation criterion. Here, samples are exclusively placed near the target contour and the remaining area remains unexplored. Consequently, the amount of samples and therefore the training effort can be reduced. It is important to note, that both contour plots indicate a smooth functional response although the number of tubes is a discrete input. These results indicate that active learning for GPR training is suitable to approximate the HEX analysis.

5.3. Training of heat exchanger surrogate models

In a recuperated Brayton cycle, three heat exchangers need to be designed. As introduced in Sections 3 and 2.3, the heat flow rate $\dot{Q}$ and pressure drops $\boldsymbol{\Delta P}$ on hot and cold side are the required functional output of the analysis. In addition to five geometric parameters, the inflow conditions of both sides are variable training parameters for the surrogate model. For the process sides of heat sink HEX (HTHX) and source HEX (LTHX) these inflows conditions are constant parameters. On HP cycle side, mass flow, temperature and total pressure are training parameters adding up to eight dimensions for HTXH and LTHX. For the recuperator, there are two more parameters, as the inflow on the secondary side is variable as well. Temperature and total pressure need to be included which adds up to 10 parameters. The mass flow rates on both sides are identical as they are both connected to the HP cycle. Offline models with individual training databases for each function are trained using GPR and the sampling strategies introduced in Section 5.1. In this work, local HEX models are applied in preparation of future studies with online adaptive models.

Fig. 12 shows the parity plots to visualize the prediction quality for the heat sink heat exchanger. 1500 test samples generated with LHS are evaluated. The scattered data compares the simulated values on the x-axis to the predicted values on the y-axis. If the prediction is perfect, simulated and predicted value are identical and the corresponding point will appear on the gray diagonal line. The quality of the model for the heat flow rate $\dot{Q}$ is shown in Fig. 12(a). It has been trained using adaptive refinement with contour estimation, as the heat flow rate is a process requirement and thereby a constant value. As a consequence, the model needs to be most accurate near this target value of 7.24 MW. Overall, a very high global accuracy is reached, even though it has been only locally refined. Near the highlighted contour value, predicted values are almost spot on. No outliers are detected. As an explanation for good global accuracy, the sensitivity of the training parameters can be considered. The heat flow rate is dominated by the inflow temperature followed by tube length and mass flow (see Fig. D.19(a)). Remaining parameters only have minor impact, which can explain why the local sensitivities also apply globally. The GPR model for tube side pressure drop in Fig. 12(b) also reaches high global accuracy and has been trained with multi contour estimation for a

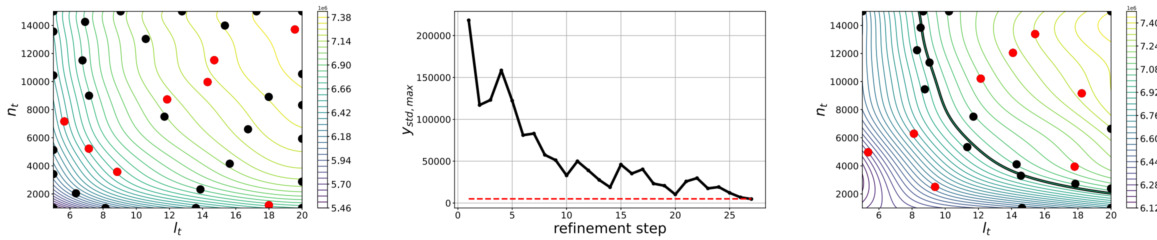

(a) (b) (c)

Fig. 11. 2D active learning test case with prediction of HEX analysis. Initial models are trained with LHS (red points) and refined until a threshold of the standard deviation $y_{\text{std, max}}$ is reached (a): Global refinement. (b): Convergence of the algorithm. (c): Local refinement for a target contour.

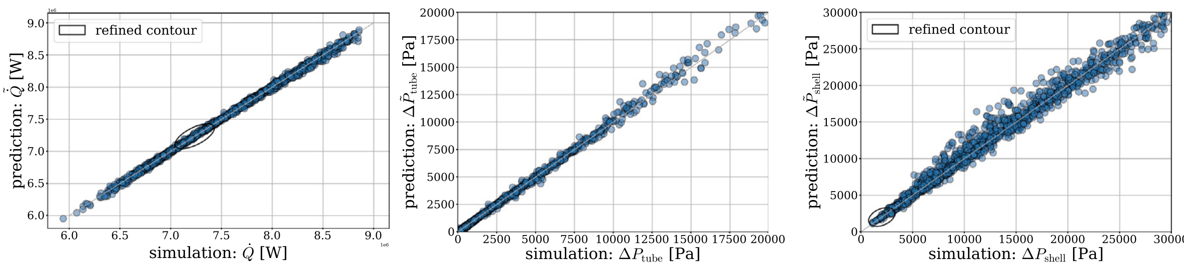

(a) (b) (c)

Fig. 12. Model accuracy of GPR for the prediction of heat sink $\dot{Q}$. Parity of simulations and model predictions with 1500 test samples (a), tube side pressure drop (b) and shell side pressure drop (c).

Table 2
Metrics to rate global model accuracy for heat exchanger surrogates.

	Sink HTHX			Source LTHX			Recuperator		
	n_{train}	R^2	$\bar{e}_{\text{abs, rel.}}$	n_{train}	R^2	$\bar{e}_{\text{abs, rel.}}$	n_{train}	R^2	$\bar{e}_{\text{abs, rel.}}$
$\dot{Q}$	45	0.998	0.25%	79	0.999	0.2%	74	0.999	0.29%
ΔP_{tube}	120	0.994	5.6%	150	0.998	3.7%	150	0.998	9.2%
ΔP_{shell}	112	0.991	7.2%	89	0.976	7.4%	150	0.992	5.3%

range of low pressure drops. As before for the prediction of $\dot{Q}$, the parameter sensitivity can explain the high global accuracy. In this case, the tube diameter is dominant followed by the number of tubes (see Fig. D.19(b)). The shell side pressure drop is visualized in Fig. 12(c). This model shows more deviation between simulated and predicted values with increasing pressure drop. It has been refined locally for the relevant lowest predictions of ΔP_s. For values outside of these refined contours, the model accuracy decreases. On the one hand side this can be explained with similar sensitivity to multiple input parameters (see Fig. D.19(c)) as well as the large output range. The function appears to be more complex and harder to predict.

Metrics for global model quality are summarized in Table 2 for all HEX. The coefficient of determination R^2 and the mean absolute relative error $\bar{e}_{\text{abs, rel.}}$ are computed with the test samples. The number of training samples n_{train} results from the determination criterion of the active learning strategy. The heat flow rates reach highest global accuracy while the database for the HTXH can be kept low with only 45 samples. LTHX and Recuperator are trained with more evaluations, which are limited to 150 samples. The recuperator model is of higher dimension, which usually requires for more training data. The tube side pressure drops reach good values even though global metrics are applied to rate the local models. This also accounts for the shell side pressure drops. The local accuracy near refined areas is potentially higher, which is evaluated with the optimized configurations in Section 6.2. Shell sides of HTHX and LTHX are connected to the process side and their pressure drops have no impact on COP and are therefore highlighted in gray. The local models are applied to investigate if there is potential for exploitation of local errors by top-level optimizers. Low approximation errors of global models have been confirmed in [30]. Even though the HEX analysis is fast, the CPU-time for optimization is reduced from 3–5 min. to 30 s when surrogates are used.

5.4. Training of compressor surrogate models

Because of the high number of design parameters and the occurrence of convergence issues, the training of compressor offline surrogates is challenging. The evaluation of a single generic compressor design can take up to 60 s as described in Section 2.2. For this reason, the number of maximum function evaluations to generate offline models is limited to 1500. This number is below the average count of top-level evaluations in non-distributed optimization [28] and should not be exceeded to enable integration of more detailed analyses in future work. For global models, LHS is used to distribute samples in the 37-dimensional parameter space. All models are trained with the identical database. Active learning with global adaptive refinement as introduced in Section 5.1 is not applicable as it takes too many evaluations to reach global exploration. The tendency to explore the borders of the parameter space first, leads to 2^D evaluations alone, before the inner space is refined. Consequently, only local models trained for the target contour of a specified pressure ratio are used as an alternative for comparison with global models. The optimal pressure ratio is unknown beforehand. An exemplary value of $\Pi_C = 4.3$ is selected for local refinement, which is based on previous results. The purpose of using this model is focused on analyzing the active learning strategy for high dimensions and its potential to detect contours and minimize the amount of costly function evaluations. In future studies, the compressor surrogates will be refined online and local contour line detection can be beneficial for multi-sample update strategies.

A set of 400 test samples is used to compare the prediction with the simulation for the pressure ratio Π_C and the efficiency η_C in Fig. 13. As expected, with the increased dimensions of the model, the overall accuracy of predicted pressure ratios is lower compared to HEX approximations in Section 5.3. This is indicated in Fig. 13(a) with the larger spread around the diagonal line and the occurrence of outliers. However, considering the complexity of the compressor analysis, the

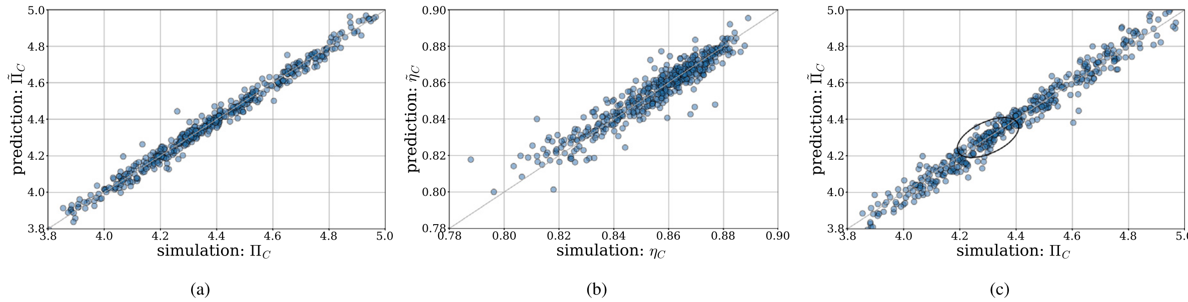

Fig. 13. Parity of GPR predictions vs. ACDC simulations. Global models for pressure ratio (a) and efficiency (b) trained with 1500 LHS samples. Local model trained with active learning for contour estimation: Prediction of the pressure ratio using 462 samples (c).

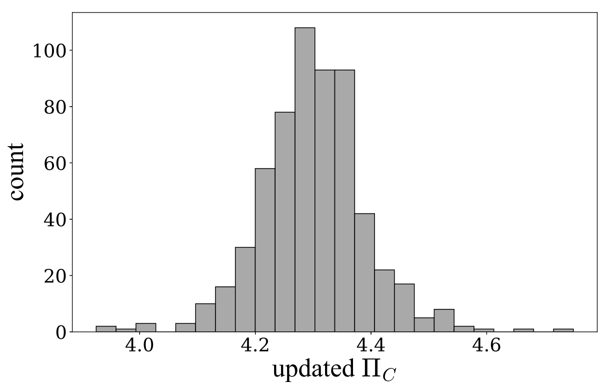

Fig. 14. Histogram with the frequency of evaluated contour values for active learning with the target contour: $\hat{\Pi}_C = 4.3$.

model accuracy appears to be high. The efficiency in Fig. 13(b) shows larger deviations while outliers appear in regions with lower values. In the relevant area of better efficiencies, a higher density close to the diagonal line indicates sufficient model quality. Larger spread compared to Π_C can be explained with the parameter sensitivity, as shown in the appendix, Fig. D.20. With the exception of p_{34}, which is the rotational speed, a variety of features evenly impact the efficiency. In comparison to that, the pressure ratio shows sensitivity to a smaller group of dominant features, which are the parameters that set the blade design of the rotors. The parity for the local model is shown in Fig. 13(c). The lower number of samples decreases global prediction quality, as expected. Near the refined contour, a higher density of accurate predictions can be observed. It should be noted that a clear effect is difficult to discern due to the high dimensionality relative to the limited number of 400 test samples.

The active learning strategy can be successfully applied, which can be seen in Fig. 14 showing the histogram of refined sample contours. A normal distribution centered around the target value is implying that the target contour $\hat{\Pi}_C = 4.3$ has been detected. An indicator for increased model accuracy near the contour line is shown in Appendix B, Fig. E.21. Averaged standard deviations near the contour value are decreased and reach similar values compared to the global model with almost 3 times the number of sample points. This result confirms, that contour line estimation can be a suitable update strategy to refine global models.

Table 3 summarizes the metrics for global model quality. Values for the GPR models to predict diffusion coefficients ($c_{d,max}$, $c_{d,min}$) and the stability criterion c_{koch} are additionally listed. The trends derived from the parity plots are confirmed: The larger database of the global model with 1500 samples leads to better coefficients of determination R^2 and tends to smaller prediction errors. Overall, the efficiency η_C alongside with c_{koch} seem to be the functions that are most challenging to predict

Table 3
Metrics for global model accuracy of compressor surrogates.

Sampling	LHS 1500 samples		CE 462 samples	
Criterion	R^2	$\bar{e}_{\text{abs, rel.}}$	R^2	$\bar{e}_{\text{abs, rel.}}$
Π_c	0.986	0.56%	0.97	0.87%
η_c	0.883	0.53%	0.78	0.75%
$c_{d,max}$	0.916	5.1%	0.89	4.4%
$c_{d,min}$	0.895	14.5%	0.85	15%
c_{koch}	0.876	1.8%	0.8	2.2%

with regard to R^2. Lower R^2 indicates larger variance and or the occurrence of outliers. Except for $c_{d,min}$, mean relative absolute errors $\bar{e}_{\text{abs, rel.}}$ are below 5.1%. In conclusion, the models show sufficient correlation between simulated and predicted data and are thereby applicable for the investigation of the holistic optimization structures. As for the HEX regressions, the analysis of local models serves as a basis to apply online refined models in future work.

6. Results and discussion

The holistic optimization structures introduced in Section 3 are investigated comparatively with regard to objective function values, convergence and stability. The results are further discussed considering generalizability of the approaches. In previous work, the AAO architecture has been analyzed in comparison to the NHX structure. The distribution of HEX optimization in NHX enables easier search for feasible configurations, as the heat exchangers are optimized for target values. Building up on this, two additional structures are investigated in this paper that fully distribute component optimizations to subproblems. Collaborative design (CD) is extended with cycle-optimized collaborative design (OCD). Distributed structures require fast evaluation of subproblems. For this reason, surrogate models replace the component analysis, as specifically the subproblem optimization of the compressor design is too costly if directly performed with the aerodynamic analysis. The surrogate models are evaluated for local prediction errors to rule out the potential exploitation of model inaccuracy by the top-level optimizers. Finally, the results are discussed and an outlook to future work is given.

6.1. Comparison of objective function values, convergence and solution similarity

The optimization concepts NHX, CD and OCD are repeated 5 times to assess their capability for holistic heat pump optimization. Fig. 15(a) shows a 2D box plot to visualize results for the spread of top-level evaluations as well as objective function value COP^* for the repeated runs. The shaded areas visualize the borders of min/max values and the black dot is the mean. Assuming normal distribution, the black lines indicate the $\mu \pm 2\,\sigma_{std}$ confidence interval. The latter means, that based on the evaluated points 95% of the results of this optimization approach are

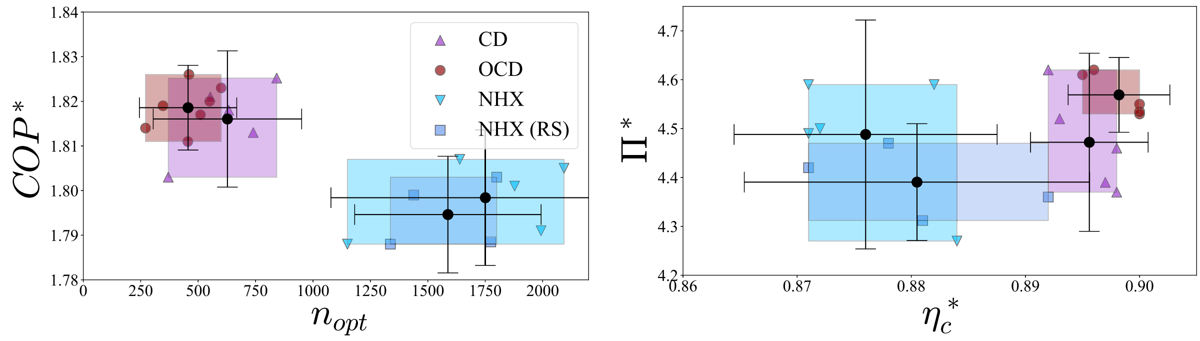

(a) (b)

Fig. 15. Two-dimensional box plots with results of repeated holistic optimizations. (a) Comparison of objective function values and number of top-level evaluations. (b) Comparison of optimized values for compressor efficiency and pressure ratio. The scattered points represent the individual evaluations and the shaded area highlights the spread. The centered black point is the mean value and the black lines indicate the 95% confidence interval.

likely to be within this range. It can be seen, that both fully distributed architectures (CD, OCD) are able to significantly reduce the top-level evaluations compared to NHX. This is because NHX performs the complex compressor design with 37 variables on top-level. To enable direct comparison, component surrogates are used in NHX (RS) leading to similar results compared to direct tool integration in NHX. There is a slight trend that the number of iterations is reduced, which can be explained with the fact that surrogate models prevent convergence issues that can occur with physics based models. The number of necessary top-level evaluations for NHX strongly depends on the first detected feasible compressor design, which is then slowly improved. This is the reason for a large spread in top-level evaluations and some deviation in the optimized objective function values. Compared to this, CD invokes better objectives and improved heat pump designs. This trend is further recognizable with the OCD structure that is able to reduce the variance of results. High objective function values are achieved with better consistency. This can be explained by the embedded cycle optimization in this structure so that the top-level optimizer mainly deals with orchestration of target values and detection of feasible regions. Fig. 15(b) shows the final, optimized compressor parameters η_C^* and Π_C^* for each run. Both CD and OCD detect compressors designs with higher efficiency compared to NHX. The NHX(RS) structure uses the identical surrogates, which excludes prediction errors as an explanation. This is a strong indicator, that distributed structures are beneficial to detect more efficient components. NHX shows a significant spread of optimized values, which is also caused by the complex compressor optimization performed on top-level. The variance of pressure ratios in the CD structure is of comparable magnitude. This is caused be the cycle parameters on top-level that require the optimizer to evaluate a wide range of mass flows which need to be matched with process flow rates and optimal component targets. As OCD deals with this as a subproblem, only two groups of results are found here with overall low variance. The subproblem optimization of the thermodynamic cycle invokes that the temperature composite curves of the heat exchangers are always matched with the process side so that mass flow and pressure ratio are always optimal. Consequently, the top-level design space is reduced as well as parameter interactions. The reproducibility of the OCD results is therefore very high. In summary, it can be stated that both distributed structures invoke improved designs while requiring less top-level evaluations. OCD is the most promising structure with highest reliability for the optimization of a recuperated Brayton cycle HP.

Fig. 16(a) shows the convergence of these compressor parameters in a single run of OCD. The top-level optimizer increases the compressor efficiency simultaneously with the adaption of the optimal pressure ratio, which are interacting parameters. As the best feasible compressor designs are found, the targets are harder to achieve, which can be seen by the bar plots in the bottom right area. These are deviation values

Table 4
Local prediction errors of optimized HEX configurations. Gray values are on process side and not relevant for cycle performance.

	$\dot{Q}$	Tube side	Shell side
	$e_{a,\dot{Q}}$	$e_{a,\Delta P_t}$	$e_{a,\Delta P_s}$
HTHX	1.5e−3	1.5e−3	5.8e−2
LTHX	1.5e−3	3.4e−2	7e-2
Recu.	2.4e−3	4.8e−2	6.3e−2

from targets and as the top-level optimizer gets closer to the globally optimal heat pump, the compressors targets approach the border of feasibility. Fig. 16(b) shows the terminal temperature difference ttd, which is the performance parameter for heat transfer in HEX, for the optimization of the recuperator. Here, the optimizer detects a high fraction of feasible designs below the acceptable deviation threshold. This can be explained with the lower dimensions, less complex function output and wide bounds compared to the compressor optimization. The HEX subproblem optimization minimizes the length l_{HEX} within the defined bounds. The search space is fully used as indicated by the scattered normalized l_{HEX} points located at the upper bound. This means that the available HEX design space is fully used by setting targets that lead to designs with high surface area enabling efficient heat transfer. In summary these findings support that the communication between top-level and subproblem optimizers is able to trace feasible and efficient component designs, which are simultaneously matched in their optimal operating points on cycle level.

6.2. Evaluation of local prediction errors

The use of offline-trained surrogates carries the risk that local prediction errors are exploited by the subproblem optimizers. This would lead to falsely predicted component parameters and consequently invoke false prediction of heat pump performance. Metrics for global evaluation of average prediction errors (see Section 5) give an indication about model quality but are very dependent on the test dataset. Specifically for locally refined models, like they are applied in this work, global evaluation needs to be supported with evaluation of local errors. In this work, local models are used in preparation for applying online refined models with similar characteristics in future studies. The prediction error $e_a = \mathrm{abs}(1 - (x/\tilde{x}))$ is defined as the relative deviation of the predicted value $\tilde{x}$ from the simulated output x. These errors are evaluated for results from OCD holistic optimizations. The optimal design parameter vector $\boldsymbol{p}^*$ for holistically optimal targets is first computed with subproblem optimization performed with the surrogates. Then, the identical $\boldsymbol{p}^*$ is evaluated with the physics based component analysis to investigate differences.

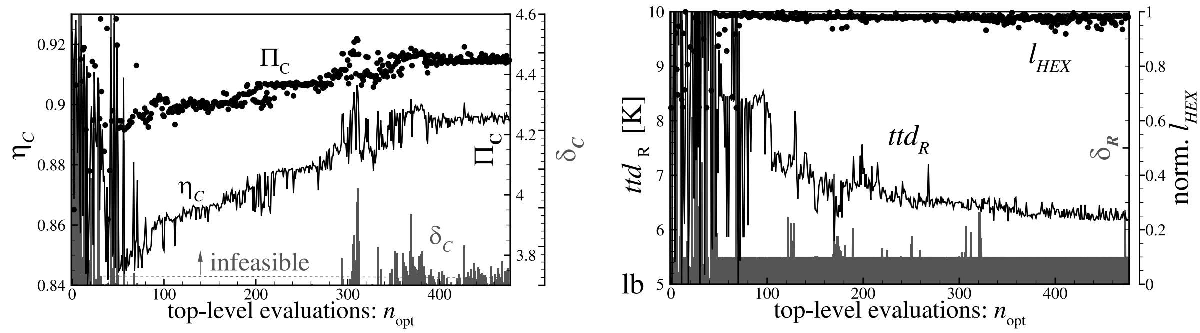

(a) (b)

Fig. 16. Convergence of component target efficiency parameters for the compressor (a) and recuperator (b) with OCD. The black lines indicate the values set as targets for distributed holistic design. The gray bars are the target deviations that are handled as constraint functions on top-level.

Table 5
Target values and local prediction errors for optimized compressor designs.

Global models	$\hat{y}^*$	$\tilde{y}^*$	e_a
η_c	0.899	0.899	1.4%
Π_C	4.6	4.6	0.04%
c_{koch}	≤ 1	1.0	8%
$c_{\text{df, max}}$	≤ 0.6	0.6	1.6%
$c_{\text{df, min}}$	≥ 0.35	0.42	7.1%
Local models	$\hat{y}^*$	$\tilde{y}^*$	e_a
η_c	0.898	0.898	2.3%
Π_C	4.534	4.534	1.2%
c_{koch}	≤ 1	0.99	4%
$c_{\text{df, max}}$	≤ 0.6	0.58	1,%
$c_{\text{df, min}}$	≥ 0.35	0.35	0.09%

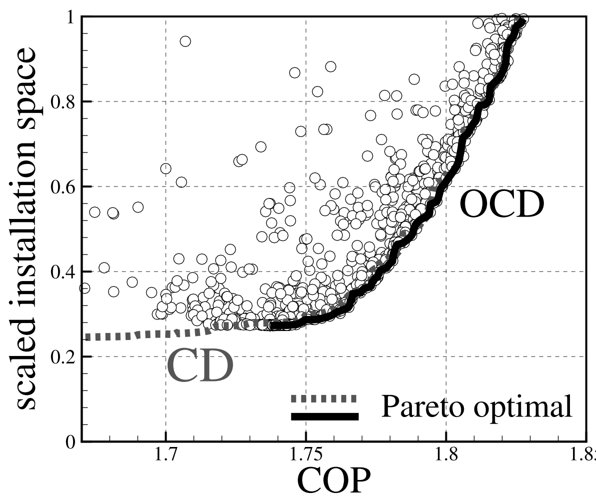

Fig. 17. Comparison of detected Pareto fronts for conflicting objectives of installation space and COP of the heat pump.

The local prediction errors e_a for the heat exchanger surrogates are summarized in Table 4. As expected, predictions for heat flow rates are spot on, which is also indicated by global metrics. The prediction errors for pressure drops are higher but a maximum value of $e_a \leq 6.3\%$ is in the acceptable range. Generally, the shell side pressure drop shows the largest deviations.

Table 5 shows the prediction errors for global and local compressor surrogates. The optimized target values for pressure ratio Π_C, efficiency η_C, stability criterion c_{koch} and extreme values of stage diffusion coefficients ($c_{\text{df, max}}$, $c_{\text{df, min}}$) are listed. For the global model, high accuracy is reached for pressure ratio and efficiency prediction. The Koch-criterion shows the largest deviations. All these models haven been trained with the identical database. Same accounts for the local model, which has been refined near a target pressure ratio contour. It uses less samples but still provides sufficient accuracy for efficiency and pressure ratio approximation. In this case, it even provides better local predictions for the stability coefficients. These results generally indicate, that the offline surrogate approach is valid if models are trained accordingly. But to mitigate the risk of local prediction errors and their exploitation, these model can be locally refined with online updates in adaptive optimization concepts. This will also result in models with locally dense samples, as applied in this study. It is shown that these are suitable to be used in the distributed holistic optimization structures with no indication of exploitation.

6.3. Discussion of holistic optimization strategies

The results of this work underline that the architecture of holistic optimization concepts is decisive for its reliable performance. Table 6 summarizes advantages and disadvantages of the considered optimization concepts. OCD is proposed as the most suitable structure. It simplifies the problem for the top-level optimizer as the cycle states are always optimized in a subproblem. Distributed structures are generalizable to any kind of heat pump cycle or integrated analysis as the subproblems just need to be formalized accordingly. These can be executed in parallel, which is why the number of integrated components is only limited by the available computing power. Distributed structures can reduce overall computational effort, which is 47 h for OCD. All optimization haven been performed using a Linux workstation with 250 GB RAM and the Intel Xeon Gold Processor 5220 with 36 cores. Direct tool integration with more costly analyses leads to high computational effort. For a fair comparison, surrogate training needs to be considered. With the fast HEX analysis, surrogates can be trained in less than 10 min. The low number of required samples indicates that higher dimensional HEX analysis could be integrated. Compressor training with 1500 samples to build global models is done in approx. 10 h. Local models with adaptive refinement can speed up the process as long as the continuous training of the surrogate does not create a bottleneck and is of similar effort than the analysis. Using surrogates has the additional advantage, that no issues with convergence can occur which is beneficial for the optimization.

The present work contributes to improve holistic design processes of closed cycle heat pumps compared to conventional approaches. The results indicate that integration of component designs can be applied with a moderate number of function evaluations even for complex analyses. Holistic concepts invoke better heat pump designs with globally balanced component performance while trial and error of sequential processes is eliminated. The design process itself will be more efficient for potential users. Communication of the exchange of targets and interface parameters of each discipline are automatized during the

Table 6
Comparative overview of investigated optimization structures.

	AAO	NHX	CD	OCD
Advantages	Easy implementation. No subproblems and fast process chains.	Focused on cycle evaluated compressor design. Improved reproducibility. With fast HEX analysis no need for surrogates.	Fast and reliable convergence rate. Distribution of problems allows generalization to all types of heat pumps.	Improves CD as the cycle is always optimized in a subproblem for component targets.
Disadvantages	Slow convergence that is highly dependent on the initial feasible solution.	Not generalizable for heat pump systems. Complex compressor design on top-level.	Surrogate models are required. Risk of exploitation of approximation errors.	Surrogate models are required. Risk of exploitation of approximation errors.
Function evaluations of analyses	Corresponds to the number of top level iterations: $n_{\text{fev}} > 5000$	Corresponds to top-level evaluations for compressors: $n_{\text{fev, C}} < 2000$. Very high for HEX subproblems.	Corresponds to training samples of surrogates: $n_{\text{fev, C}} < 1500$ $n_{\text{fev, HEX}} < 150$	Corresponds to training samples of surrogates: $n_{\text{fev, C}} < 1500$ $n_{\text{fev, HEX}} < 150$
CPU time 1: tool integration 2: surrogates	1: $t_{\text{CPU}} \approx 100\,\text{h}$ 2: n. a.	1: $t_{\text{CPU}} \approx 200\,\text{h}$ 2: $t_{\text{CPU}} \approx 10\,\text{h}$	1: n.a. 2: $t_{\text{CPU}} \approx 40\,\text{h}$	1: n.a. 2: $t_{\text{CPU}} \approx 47\,\text{h}$

optimization process. This helps to save time and avoid mistakes. It also helpful, that geometric information is available throughout the earliest phases of design. Consideration of additional objectives like engine size, installation space, weight and costs is beneficial for decision making and constraining designs. An example for this is shown in Fig. 17 comparing multi-objective results for the trade-off between heat pump performance and installation space, which is quantified with HEX length:

$$\min_{p} \left[-COP,\ \max\{l_j\}\right] \tag{37}$$

Both distributed structures (OCD, CD) are able to capture the identical Pareto front supporting the validity of these optimization concepts. The scattered data points are the $n_{\text{opt}} \approx 1000$ OCD evaluations.

6.4. Limitations

Potential has been shown, but limitations of the proposed concept need to be considered. First, although the modular characteristic using surrogates in distributed approaches allows the integration of all kinds of simulation tools, a one-button approach to optimize a heat pump in a single process, without the need for subsequent design steps, has not yet been demonstrated. Holistic optimizations currently use preliminary design methods for an improved conceptual design. The benefits of this have been underlined in this paper, but additional steps with detailed CFD-based component design are still necessary. The potential for integrating CFD methods will depend on the computational training effort required to predict functional outputs with surrogates. Another limiting aspect is currently the consideration of off-design performance in holistic design. This will require predicting the part-load behavior of each component design to be evaluated at the cycle level. This is a major development step, and there are several conceivable methods to approach this. Preliminary methods can be integrated with the cycle solver, either directly or through robust matching of component maps, which has been demonstrated for ACDC [59]. Higher-fidelity methods like CFD will require prediction approaches to approximate off-design performance in order to avoid excessive computational effort. In the case of closed-cycle Brayton heat pumps, considering only the design point is a valid assumption, as concepts like fluid inventory control allow for part-load operation while aerodynamic conditions in turbomachines remain similar [31].

6.5. Outlook and future work

There remains substantial potential for further investigations in holistic heat pump optimization. Whether through new cycles, variation of integrated analyses, or the exploration of suitable optimization algorithms and regression methods, numerous opportunities exist for future research. Computational effort can potentially be further reduced with minor improvements like using optimized designs as initialization in subsequent iterations. Alternative training strategies for surrogates with pre-optimized designs are conceivable, which would speed up the holistic optimization but drastically increase training effort. A portfolio approach could be pursued with holistic architectures using a collection of commercially available or previously optimized designs for technology selection. Future research building up on the main findings of this paper will focus on two aspects: As a straightforward step, the integration of turbine design will be demonstrated with a suitable analysis. This will be an additional subproblem in distributed approaches. As part of the current work, the integration of turbine meanline analysis has proven to be compatible with the proposed optimization concept, as expected. Secondly, the holistic optimization strategy will be adapted to use online refined surrogates. During the optimization, initially trained coarse surrogates will be refined in areas the top-level optimizer is directing the design points. Using local surrogates in this paper is a preparatory step. Contour estimation can be applied as a potential multi-sample update strategy. These online updates will reduce the risk of local approximation errors. The findings of this work indicate moderate training effort for the implemented surrogates, which is why future studies will also analyze holistic optimization with high-dimensional modeling like CFD. Another future direction is the consideration of multiple operating points. Automatizing the procedure for cycle off-design evaluation is challenging, as discussed in Section 6.4.

7. Conclusions

This paper gives a detailed, comparative analysis of four different optimization architectures for holistic, multidisciplinary design of Brayton cycle heat pumps. The optimization of thermodynamic cycle parameters is performed simultaneously with the complex multistage compressor design and geometric sizing of three heat exchangers. Single- and multi-objective optimizations are investigated. Overall, $\boldsymbol{p} \in \mathbb{R}^{[59,60]}$ design parameters are optimized, which exceeds comparable studies that are usually restricted to integrated meanline compressor design ($\boldsymbol{p} \in \mathbb{R}^{<20}$). Geometric information enables additional objectives, specifically engine size, installation space, weight or costs. The design process itself will be more efficient and reliable, bringing together individuals and departments in automatically coordinated processes. The main findings can be summarized as follows:

1. Component performance has a large impact on the COP and the optimal pressure ratio of the heat pump. Consequently, there are interactions and the cycle design benefits from integrated

component optimization to reach globally optimal results while avoiding the risk of infeasible component configurations.
2. Distributed structures with subproblem optimizations are beneficial for convergence rates and reliability, reducing the number of top-level iterations from about 2000 to less than 500 compared to non-distributed concepts.
3. To integrate complex models, collaborative structures require surrogates for the repetitive subproblem optimizations to reduce numerical effort. Local Gaussian process surrogate models are suitable for approximating the complex function output of both compressor and heat exchanger analysis.
4. Function evaluations for surrogate training can be kept below 150 for heat exchangers per predicted function and less than 1500 for the 35 dimensional compressor analysis.
5. The proposed cycle-optimized collaborative design structure leads to the best objective function values and the fastest convergence, with high reproducibility of results, including similar optimal compressor parameters such as target pressure ratios, efficiency and mass flow rates.
6. The modular structure of the proposed holistic optimization concept will be applicable to all types of heat pump cycles and together with the reduced number of function evaluations potentially allows to integrate high dimensional models.
7. A Brayton cycle heat pump with a second-law efficiency of 80% can be optimized from scratch in less than 50 CPU hours. A COP of 1.82 is attainable with a temperature lift of 260 K, underlining the potential of very high temperature heat pumps.

This work advances holistic optimization strategies independent of cycle architecture and integrated models, enabling more efficient and reliable designs of future industrial heat pumps. As an outlook, distributed structures will be further analyzed using adaptive online-trained surrogate models to mitigate the risk of local approximation errors.

Declaration of competing interest

The authors declare that they have no known competing financial interests or personal relationships that could have appeared to influence the work reported in this paper.

Appendix A. Thermodynamic cycle modeling

The basic state change equations for all relevant components are listed in Table A.7:

Table A.7
State-change equations for Brayton heat pumps. Steady-state mass and energy balance.

Component	Mass balance	Energy balance
Compressor	$\dot{m}_1 = \dot{m}_2$	$\dot{W}_c = \dot{m}_1(h_2 - h_1)$ $\Pi_C = p_2/p_1$ $h_{2,s} = h(p_2, s = s_1)$ $h_2 = \frac{h_{2,s} - h_1}{\eta_c} + h_1$
Turbine	$\dot{m}_4 = \dot{m}_5$	$\dot{W}_t = \dot{m}_4(h_4 - h_5)$ $\Pi_T = p_5/p_4$ $h_{5,s} = h(p_5, s = s_4)$ $h_5 = h_4 - \eta_t(h_4 - h_{5,s})$
Heat exchangers	$\dot{m}'_{in} = \dot{m}'_{out}\dot{m}''_{in} = \dot{m}''_{out}$	$\dot{Q} = \dot{m}'(h'_{in} - h'_{out})$ $\dot{Q} = \dot{m}''(h^{('')}_{out} - h''_{in})$ $T'_{in} - T''_{in} \geq T_{ttd,min}$ $T''_{out} - T'_{out} \geq T_{ttd,min}$

Table A.8
Boundary conditions for holistic heat pump optimization study.

Boundary condition	Value
heat sink (process side)	
$\dot{m}_9$	32 kg/s
T_9	100°C
T_{10}	320°C
heat source (process side)	
$\dot{m}_7$	35 kg/s
T_7	60°C
T_8	var.
cycle parameters	
p_1	1.013×10^5 Pa
η_T	0.93

The boundary conditions $\boldsymbol{c}_{cyc}$ for the case study are summarized in Table A.8. All remaining cycle states are computed based on the component performance parameters derived from integrated component analyses. The parameterization of the thermodynamic cycle evaluation in Tespy depends on its interfaces to integrated tools. In general, the component performance parameters in $\boldsymbol{p}_{cyc}$ need to be accessible. The temperature requirements are chosen to match the pressure ratio range of the 4-stage axial compressor.

Appendix B. Heat exchanger correlations

P-NTU method and effectiveness
Tube-side heat transfer: Nusselt correlation [60]

$$\mathrm{Nu} = \begin{cases} 0.0214\left(\mathrm{Re}^{0.8} - 100\right)\mathrm{Pr}^{0.4}\left(1 + \left(\frac{D}{L}\right)^{\frac{2}{3}}\right), & \text{if } \mathrm{Pr} \leq 1.5 \\ 0.012\left(\mathrm{Re}^{0.87} - 280\right)\mathrm{Pr}^{0.4}\left(1 + \left(\frac{D}{L}\right)^{\frac{2}{3}}\right), & \text{if } \mathrm{Pr} > 1.5 \end{cases} \tag{B.1}$$

$$\alpha = \frac{\mathrm{Nu}\cdot k}{D} \tag{B.2}$$

Shell-side heat transfer [61].

$$\mathrm{Nu}_{lam} = 0.664\sqrt{\mathrm{Re}}\,\mathrm{Pr}^{1/3} \tag{B.3}$$

$$\mathrm{Nu}_{turb} = \frac{0.037\,\mathrm{Re}^{0.8}\,\mathrm{Pr}}{1 + 2.443\,\mathrm{Re}^{-0.1}\left(\mathrm{Pr}^{2/3} - 1\right)} \tag{B.4}$$

$$\mathrm{Nu}_0 = 0.3 + \sqrt{\mathrm{Nu}_{lam}^2 + \mathrm{Nu}_{turb}^2} \tag{B.5}$$

$$f_a = \begin{cases} 1 + \frac{0.7(b/a - 0.3)}{\psi^{1.5}\left[(b/a) + 0.7\right]^2}, & \text{square pitch} \\ 1 + \frac{2}{3b}, & \text{triangular pitch} \end{cases} \tag{B.6}$$

$$\mathrm{Nu} = f_a\,\mathrm{Nu}_0 \tag{B.7}$$

$$\alpha = \frac{\mathrm{Nu}\cdot k}{D_o \cdot 0.5 \cdot \pi} \tag{B.8}$$

$$kA = \left(\frac{1}{\alpha_i A_i} + \frac{1}{\alpha_a A_a} + \frac{\delta}{k_w A_m}\right)^{-1} \tag{B.9}$$

$$\mathrm{NTU} = \frac{kA}{\dot{m}c_p} \tag{B.10}$$

$$P = \begin{cases} \dfrac{\mathrm{NTU} \cdot f}{1 + \mathrm{NTU} \cdot f}, & \text{if } R = 1 \\ \dfrac{1 - \exp\left[(R-1) \cdot \mathrm{NTU} \cdot f\right]}{1 - R \cdot \exp\left[(R-1) \cdot \mathrm{NTU} \cdot f\right]}, & \text{otherwise} \end{cases} \tag{B.11}$$

$$\Delta T = T_{t,\mathrm{in}} - T_{s,\mathrm{in}} \tag{B.12}$$

$$T_{s,\mathrm{out}} = T_{s,\mathrm{in}} + P_s \Delta T \tag{B.13}$$

$$T_{t,\mathrm{out}} = T_{t,\mathrm{in}} - P_t \Delta T \tag{B.14}$$

$$Q_s = \dot{m}_s c_{p,s} (T_{s,\mathrm{out}} - T_{s,\mathrm{in}}) \tag{B.15}$$

$$Q_t = \dot{m}_t c_{p,t} (T_{t,\mathrm{out}} - T_{t,\mathrm{in}}) \tag{B.16}$$

Tube-side pressure loss [62].

$$\Delta p_T = \zeta_T \frac{l}{d_T^{(i)}} \frac{\rho u^2}{2}, \quad \zeta_T = \frac{0.3164}{\sqrt[4]{\mathrm{Re}_T}}.$$

Shell-side pressure drop in cross-flow tube bundles [62] L1-5.

$$f_{zl} = \left(\frac{\mu_w}{\mu}\right)^{\frac{0.57}{\left[\left(\frac{4ab}{\pi} - 1\right)\mathrm{Re}\right]^{0.25}}} \tag{B.17}$$

$$f_{zt} = \left(\frac{\mu_w}{\mu}\right)^{0.14} \tag{B.18}$$

$$f_{\alpha l} = \begin{cases} \dfrac{280\pi \left[\left(\sqrt{b} - 0.6\right)^2 + 0.75\right]}{(4ab - \pi)\, a^{1.6}}, & \text{square} \\ \dfrac{280\pi \left[\left(\sqrt{b} - 0.6\right)^2 + 0.75\right]}{(4ab - \pi)\, a^{1.6}}, & b > 0.5\sqrt{2a+1} \\ \dfrac{280\pi \left[\left(\sqrt{b} - 0.6\right)^2 + 0.75\right]}{(4ab - \pi)\, c^{1.6}}, & \text{otherwise} \end{cases} \tag{B.19}$$

$$\zeta_l = \frac{f_{\alpha l}}{\mathrm{Re}} \tag{B.20}$$

$$f_{\alpha t} = \begin{cases} \left(0.22 + \dfrac{1.2\left(1 - \frac{0.94}{b}\right)^{0.6}}{(a - 0.85)^{1.3}}\right) 10^{0.47\left(\frac{b}{a} - 1.5\right)} + 0.03(a-1)(b-1), \\ 2.5 + \dfrac{1.2}{(a - 0.85)^{1.08}} + 0.4\left(\frac{b}{a} - 1\right)^3 - 0.01\left(\frac{a}{b} - 1\right)^3 \; \text{triangular} \end{cases} \tag{B.21}$$

$$\zeta_t = \begin{cases} \dfrac{f_{\alpha t}}{\mathrm{Re}^{0.1\, b/a}}, & \text{square} \\ \dfrac{f_{\alpha t}}{\mathrm{Re}^{0.25}} \end{cases} \tag{B.22}$$

$$\zeta = \begin{cases} \zeta_l f_{zl} + \zeta_t f_{zt} \left(1 - \exp\left[-\dfrac{\mathrm{Re} + 1000}{2000}\right]\right), \\ \zeta_l f_{zl} + \zeta_t f_{zt} \left(1 - \exp\left[-\dfrac{\mathrm{Re} + 200}{1000}\right]\right) \; \text{triangular} \end{cases} \tag{B.23}$$

$$\Delta p_{\mathrm{cross}} = \zeta n_w \rho \frac{u_m^2}{2} \tag{B.24}$$

$$\gamma = 2 \arccos\left(1 - \frac{2h_w}{D_b}\right) \tag{B.25}$$

$$A_{fg} = \frac{\pi}{4} D_s^2 \frac{\gamma}{2\pi} - \frac{D_b(D_b - 2h_w)}{4} \sin\left(\frac{\gamma}{2}\right) \tag{B.26}$$

$$A_{fr} = \frac{\pi}{4} d_o^2 \frac{N_f}{2}, \quad A_f = A_{fg} - A_{fr} \tag{B.27}$$

$$P_w = \pi D_s \frac{\gamma}{2\pi} + \pi d_o \frac{N_f}{2}, \quad d_h = \frac{4A_f}{P_w} \tag{B.28}$$

$$u_p = \frac{\dot{m}_S}{\rho_S A_f}, \quad u_z = \sqrt{u_S u_p} \tag{B.29}$$

$$(\Delta p_{ft})^2 = \left(0.6 N_{wf} + 2\right) \frac{\rho_S u_z^2}{2} \tag{B.30}$$

$$\Delta p_{\mathrm{window}} = \sqrt{(\Delta p_{fl})^2 + (\Delta p_{ft})^2}\, f_{zt} f_{zl} \tag{B.31}$$

$$\Delta p_S = \begin{cases} \left(N_b + 1\right) \Delta p_{\mathrm{cross}} + N_b \Delta p_{\mathrm{window}} \\ \left(N_b - 1\right) \Delta p_{\mathrm{cross}} + N_b \Delta p_{\mathrm{window}} + \Delta p_{\mathrm{endzone}} \end{cases} \tag{B.32}$$

Appendix C. Compressor design framework

Excerpt from ACDC documentation: The throughflow solver is based on radial equilibrium equations and mass balances as proposed by Denton [63]:

$$\frac{d}{dq}\left(\frac{v_m^2}{2}\right) = \underbrace{\frac{dh_t}{dq}}_{I} - \underbrace{T\frac{ds}{dq}}_{II} - \underbrace{\frac{1}{2r^2}\frac{d(r^2 v_\theta^2)}{dq}}_{III} + \underbrace{\frac{v_m^2}{r_C}\sin\alpha}_{IV} + \underbrace{v_m \frac{dv_m}{dm}\cos\alpha}_{V}. \tag{C.33}$$

The terms I–III assume that the total enthalpy h_t, the entropy s, and the specific angular momentum rv_θ are known for the current computational plane. By numerically integrating this differential equation along the computational plane, the distribution of the meridional velocity v_m can be determined up to an integration constant. In this process, the curvature of the streamline surfaces is included through the radius of curvature R_m (term IV), which is why the method is referred to as the streamline curvature method. Term V contains the derivative of the meridional velocity along the stream surface. The velocity distribution must additionally fulfill the continuity condition:

$$\dot{m} = \int_{\mathrm{hub}}^{\mathrm{casing}} 2\pi \rho v_m \sin\alpha (1 - b) dq \tag{C.34}$$

where denotes the compressor mass flow and represents the local blockage. ACDC uses its own pre-optimized profile family so that profiles are allocated for the flow conditions resulting from streamline curvature simulation. For blade losses and outflow angles, a neural network is trained using a correlation framework and data from 2000 optimized airfoils [34]. Three-dimensional flow effects are considered using empirical models for tip and secondary losses. A detailed overview can be found in the dissertation by Schnoes [64].

ACDC is adapted for the use in holistic heat pump optimization with the generic design framework in Fig. C.18. Compressors can be designed from scratch with minimal user input using automated scaling and user-defined reference stage geometries.

Appendix D. Sensitivity analysis

These figures show the feature importance for heat exchanger and compressor surrogate models.

Appendix E. Standard deviations of compressor surrogates

See Fig. E.21.

Data availability

Data will be made available on request.

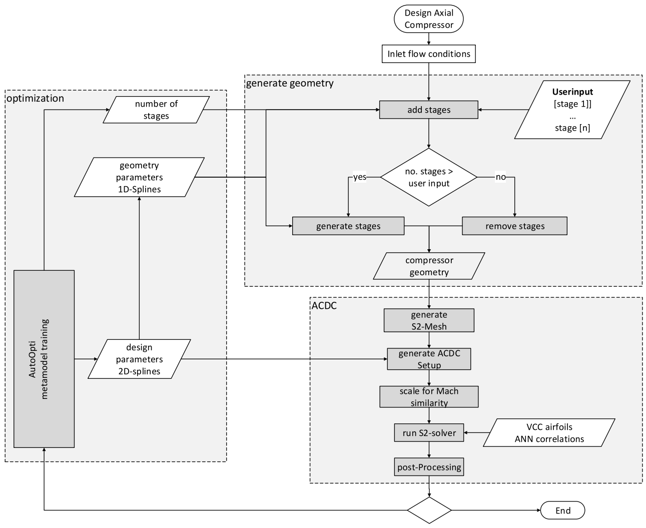

Fig. C.18. Compressor design framework for integration in holistic heat pump design.

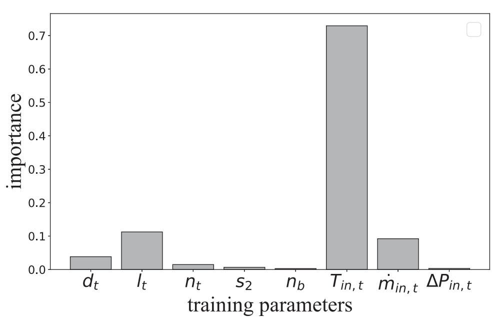

(a) Heat flow rate

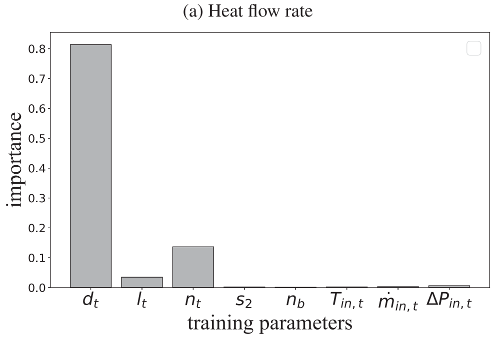

(b) Tube side pressure drop

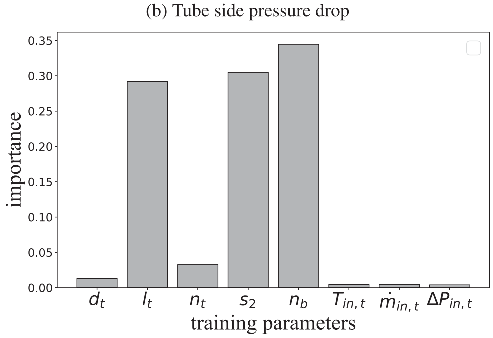

(c) Shell side pressure drop

Fig. D.19. Feature importance for HTHX model training (5000 samples, random forest).

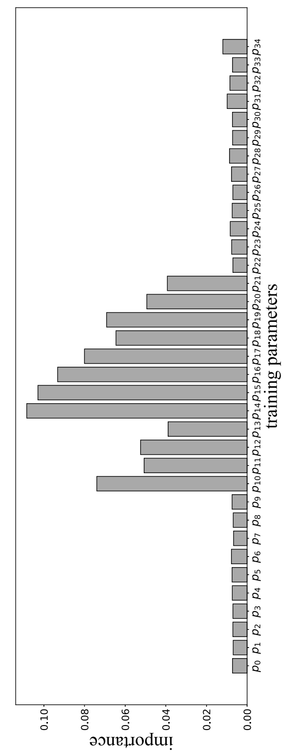

(a) Pressure ratio

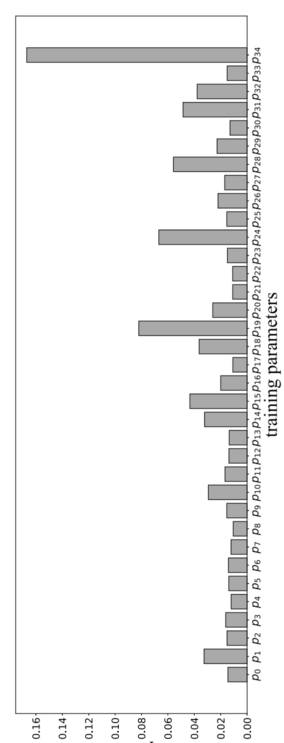

(b) Isentropic efficiency

Fig. D.20. Feature importance for compressor model (8000 samples, random forest).

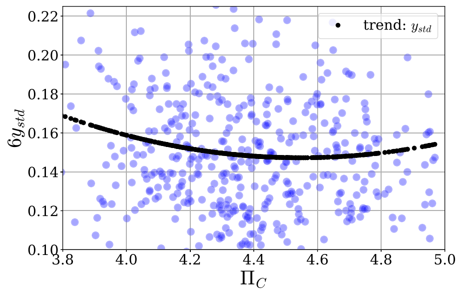

(a)

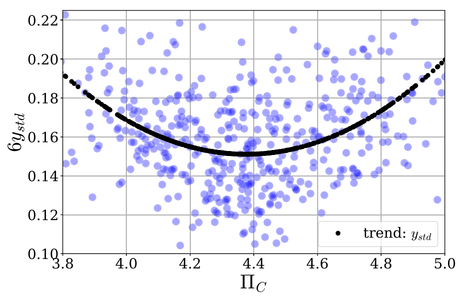

(b)

Fig. E.21. Comparison of 6-sigma interval for local and global sampling strategies. (a) Global model. (b) Local model.

References

[1] P.-M. Bever, F. Bless, C. Arpagaus, S.S. Bertsch, High–temperature heat pumps for industrial use, Chem. Ing. Tech. (2024) http://dx.doi.org/10.1002/cite.202300241.

[2] G. Kosmadakis, C. Arpagaus, P. Neofytou, S. Bertsch, Techno-economic analysis of high-temperature heat pumps with low-global warming potential refrigerants for upgrading waste heat up to 150 ° c, Energy Convers. Manage. 226 (2020) 113488, http://dx.doi.org/10.1016/j.enconman.2020.113488.

[3] J. Gollasch, M. Kriese, J. Siegel, N. Kabat, J. Walden, Numerical investigation of a heat pump demonstrator for partial electrification of the steam supply for paper drying, Appl. Therm. Eng. 278 (2025) 126941, http://dx.doi.org/10.1016/j.applthermaleng.2025.126941.

[4] L. Wang, X. Lin, H. Zhang, L. Peng, H. Chen, Brayton-cycle-based pumped heat electricity storage with innovative operation mode of thermal energy storage array, Appl. Energy 291 (2021) 116821, http://dx.doi.org/10.1016/j.apenergy.2021.116821.

[5] M. Benvenuti, G.F. Frate, L. Ferrari, Trade-off between COP and heat production temperature in high-temperature brayton heat pumps, Energy Convers. Manage. 346 (2025) 120509, http://dx.doi.org/10.1016/j.enconman.2025.120509.

[6] J. Yoo, C.E. Estrada-Perez, B.-H. Choi, Investigation of heat pump technologies for high-temperature applications above 250 ° c, Appl. Energy 384 (2025) 125384, http://dx.doi.org/10.1016/j.apenergy.2025.125384.

[7] G.F. Frate, M. Benvenuti, L. Ferrari, Multi-objective optimised preliminary design of centrifugal compressors for brayton high-temperature heat pumps, Energy Convers. Manage. 349 (2026) 120881, http://dx.doi.org/10.1016/j.enconman.2025.120881.

[8] J.R.R.A. Martins, A.B. Lambe, Multidisciplinary design optimization: A survey of architectures, AIAA J. 51 (9) (2013) 2049–2075, http://dx.doi.org/10.2514/1.J051895.

[9] R. Braun, P. Gage, I. Kroo, I. Sobieski, Implementation and performance issues in collaborative optimization, in: 6th Symposium on Multidisciplinary Analysis and Optimization, American Institute of Aeronautics and Astronautics, Reston, Virigina, 1996, http://dx.doi.org/10.2514/6.1996-4017.

[10] I. Kroo, S. Altus, R. Braun, P. Gage, I. Sobieski, Multidisciplinary optimization methods for aircraft preliminary design, in: 5th Symposium on Multidisciplinary Analysis and Optimization, http://dx.doi.org/10.2514/6.1994-4325, arXiv:https://arc.aiaa.org/doi/pdf/10.2514/6.1994-4325.

[11] A.-V. DeMiguel, W. Murray, An analysis of collaborative optimization methods, in: 8th Symposium on Multidisciplinary Analysis and Optimization, American Institute of Aeronautics and Astronautics, Reston, Virigina, 2000, http://dx.doi.org/10.2514/6.2000-4720.

[12] N.M. Alexandrov, R.M. Lewis, Analytical and computational aspects of collaborative optimization, NASA Langley Tech. Rep. Serv. (2000).

[13] I.P. Sobieski, I.M. Kroo, Collaborative optimization using response surface estimation, AIAA J. 38 (10) (2000) 1931–1938, http://dx.doi.org/10.2514/2.847.

[14] J. Tacconi, W.P.J. Visser, D. Verstraete, Multi-objective optimisation of semi-closed cycle engines for high-altitude UAV propulsion, Aeronaut. J. 123 (1270) (2019) 1938–1958, http://dx.doi.org/10.1017/aer.2019.62.

[15] M. Hendler, M. Lockan, D. Bestle, P. Flassig, Component-specific preliminary engine design taking into account holistic design aspects, Int. J. Turbomach. Propuls. Power 3 (2) (2018) 12, http://dx.doi.org/10.3390/ijtpp3020012.

[16] R. Persky, E. Sauret, L. Ma, Optimisation methods for coupled thermodynamic and 1D design of radial-inflow turbines, in: ASME 2014 4th Joint US-European Fluids Engineering Division Summer Meeting Collocated with the ASME 2014 12th International Conference on Nanochannels, Microchannels, and Minichannels, American Society of Mechanical Engineers, 2014, http://dx.doi.org/10.1115/FEDSM2014-21665.

[17] M. Lampe, C. de Servi, J. Schilling, A. Bardow, P. Colonna, Toward the integrated design of organic rankine cycle power plants: A method for the simultaneous optimization of working fluid, thermodynamic cycle, and turbine, J. Eng. Gas Turbines Power 141 (11) (2019) http://dx.doi.org/10.1115/1.4044380.

[18] S. Bahamonde, M. Pini, C. de Servi, A. Rubino, P. Colonna, Method for the preliminary fluid dynamic design of high-temperature mini-organic rankine cycle turbines, J. Eng. Gas Turbines Power 139 (8) (2017) http://dx.doi.org/10.1115/1.4035841.

[19] S. Schuster, C.N. Markides, A.J. White, Design and off-design optimisation of an organic rankine cycle (ORC) system with an integrated radial turbine model, Appl. Therm. Eng. 174 (2020) 115192, http://dx.doi.org/10.1016/j.applthermaleng.2020.115192.

[20] A. Meroni, B. Zühlsdorf, B. Elmegaard, F. Haglind, Design of centrifugal compressors for heat pump systems, Appl. Energy 232 (2018) 139–156, http://dx.doi.org/10.1016/j.apenergy.2018.09.210.

[21] A. Giuffre', F. Ascione, C. de Servi, M. Pini, Data-driven modeling of high-speed centrifugal compressors for aircraft environmental control systems, Int. J. Refrig. 151 (2023) 354–369, http://dx.doi.org/10.1016/j.ijrefrig.2023.03.019.

[22] A. Giuffre', F. Ascione, P. Colonna, C. de Servi, Integrated design optimization of environmental control systems for next-generation aircraft, J. Aircr. 2025 // 62 (3) (2025) 1–18, http://dx.doi.org/10.2514/1.C038093.

[23] F. Ascione, P. Colonna, C.M. de Servi, Integrated design optimization method for novel vapour-compression-cycle-based environmental control systems, Appl. Therm. Eng. 2024 // 236 (2024) 121261, http://dx.doi.org/10.1016/j.applthermaleng.2023.121261.

[24] F. Beltrame, P. Colonna, C.M. de Servi, Optimal design of aircraft thermal systems and their heat exchangers leveraging a data-driven surrogate model, Int. J. Heat Mass Transfer 253 (2025) 127502, http://dx.doi.org/10.1016/j.ijheatmasstransfer.2025.127502.

[25] R. Schaffrath, P. Stathopoulos, A. Schmitz, E. Nicke, Multistage turbomachinery optimization for high-temperature heat pumps with the reverse rankine cycle, J. Turbomach. 147 (11) (2025) http://dx.doi.org/10.1115/1.4068480.

[26] Y. Yan, F. Yang, H. Zhang, N. Wang, Y. Xu, J. Cheng, Z. Ge, J. Li, A holistic design framework of centrifugal compressors for high temperature heat pumps considering wet compression prevention and global optimization, Energy Convers. Manage. 342 (2025) 120142, http://dx.doi.org/10.1016/j.enconman.2025.120142.

[27] J. Gollasch, M. Lockan, P. Stathopoulos, E. Nicke (Eds.), Multi-Disciplinary Optimization of Thermodynamic Cycles for Large-Scale Heat Pumps With Simultaneous Component Design, 2023, http://dx.doi.org/10.1115/GT2023-101983.

[28] J. Gollasch, M. Lockan, P. Stathopoulos, E. Nicke, Multidisciplinary optimization of thermodynamic cycles for large-scale heat pumps with simultaneous component design, J. Eng. Gas Turbines Power 146 (2) (2024) http://dx.doi.org/10.1115/1.4063637.

[29] J. Gollasch, M. Lockan, A comparative study of component surrogate model approximation for holistic, multi-disciplinary optimization of high temperature heat pumps, in: Volume 4: Controls, Diagnostics & Instrumentation; Cycle Innovations; Education; Electric Power, American Society of Mechanical Engineers, 2025, http://dx.doi.org/10.1115/GT2025-152774.

[30] J. Gollasch, M. Lockan, A comparative study of component surrogate model approximation for holistic, multi-disciplinary optimization of high temperature heat pumps // a comparative study of component surrogate model approximation for holistic, multidisciplinary optimization of high temperature heat pumps, J. Eng. Gas Turbines Power 148 (5) (2026) 1–38, http://dx.doi.org/10.1115/1.4069927.

[31] J. Oehler, J. Gollasch, A.P. Tran, E. Nicke, Part load capability of a high temperature heat pump with reversed brayton cycle, in: 13th IEA Heat Pump Conference, 2021.

[32] F. Witte, I. Tuschy, TESPy: Thermal engineering systems in python, J. Open Source Softw. 5 (49) (2020) 2178, http://dx.doi.org/10.21105/joss.02178.

[33] E.N. Markus Schnoes, Exploring a database of optimal airfoils for axial compressor design: ISABE-2017-21493, 2017, ISABE 2017.

[34] M. Schnoes, C. Voß, E. Nicke, Design optimization of a multi-stage axial compressor using throughflow and a database of optimal airfoils, J. Glob. Power Propuls. Soc. 2 (2018) W5N91I, http://dx.doi.org/10.22261/JGPPS.W5N91I.

[35] C.C. Koch, Stalling pressure rise capability of axial flow compressor stages, ASME J. Eng. Power Vol. 103/645 (1981).
[36] D. Schönweitz, M. Voges, G. Goinis, G. Enders, E. Johann, Experimental and numerical examinations of a transonic compressor-stage with casing treatment, in: Turbo Expo, Volume 6A: Turbomachinery, 2013, http://dx.doi.org/10.1115/GT2013-95550, V06AT35A035.
[37] M. Schnoes, E. Nicke, Automated calibration of compressor loss and deviation correlations, Proc. ASME Turbo Expo 2015: Turbine Tech. Conf. Expo. (2015).
[38] Springer-Verlag GmbH, VDI-Wärmeatlas, Springer Berlin Heidelberg, Berlin, Heidelberg, 2013, http://dx.doi.org/10.1007/978-3-642-19981-3.
[39] Caleb Bell and Contributors, Ht: Heat transfer component of chemical engineering design library (ChEDL), 2016-2024, URL https://github.com/CalebBell/ht.
[40] Y.A. Çengel, A.J. Ghajar, Heat and Mass Transfer: Fundamentals & Applications, fifth ed., McGraw-Hill Education, New York, NY, 2015.
[41] C. Voß, M. Aulich, T. Raitor, Metamodel assisted aeromechanical optimization of a transonic centrifugal compressor, in: ISROMAC 15, 2014.
[42] R. Storn, K. Price, Differential evolution: A simple and efficient heuristic for global optimization over continuous spaces, J. Global Optim. 11 (1996) 341–359.
[43] P. Virtanen, R. Gommers, T.E. Oliphant, M. Haberland, T. Reddy, D. Cournapeau, E. Burovski, P. Peterson, W. Weckesser, J. Bright, S.J. van der Walt, M. Brett, J. Wilson, K.J. Millman, N. Mayorov, A.R.J. Nelson, E. Jones, R. Kern, E. Larson, C.J. Carey, İ. Polat, Y. Feng, E.W. Moore, J. VanderPlas, D. Laxalde, J. Perktold, R. Cimrman, I. Henriksen, E.A. Quintero, C.R. Harris, A.M. Archibald, A.H. Ribeiro, F. Pedregosa, P. van Mulbregt, Scipy 1.0: fundamental algorithms for scientific computing in python, Nature Methods 17 (3) (2020) 261–272, http://dx.doi.org/10.1038/s41592-019-0686-2.
[44] M.D. Morris, Factorial sampling plans for preliminary computational experiments, Technometrics 33 (2) (1991) 161–174, http://dx.doi.org/10.1080/00401706.1991.10484804.
[45] J. Herman, W. Usher, Salib: An open-source python library for sensitivity analysis, J. Open Source Softw. 2 (9) (2017) 97, http://dx.doi.org/10.21105/joss.00097.
[46] T. Iwanaga, W. Usher, J. Herman, Toward salib 2.0: Advancing the accessibility and interpretability of global sensitivity analyses, Socio-Environmental Syst. Model. 4 (2022) 18155, http://dx.doi.org/10.18174/sesmo.18155.
[47] P. Ramu, P. Thananjayan, E. Acar, G. Bayrak, J.W. Park, I. Lee, A survey of machine learning techniques in structural and multidisciplinary optimization, Struct. Multidiscip. Optim. 65 (9) (2022) http://dx.doi.org/10.1007/s00158-022-03369-9.
[48] C.E. Rasmussen, Gaussian processes for machine learning, in: Adaptive computation and machine learning series, MIT Press, Cambridge, Massachusetts, 2006.
[49] A.I.J. Forrester, A. Sóbester, A.J. Keane, Engineering Design Via Surrogate Modelling: A Practical Guide, J. Wiley, Chichester West Sussex England and Hoboken NJ, 2008.
[50] L. Buitinck, G. Louppe, M. Blondel, F. Pedregosa, A. Mueller, O. Grisel, V. Niculae, P. Prettenhofer, A. Gramfort, J. Grobler, R. Layton, J. VanderPlas, A. Joly, B. Holt, G. Varoquaux, API design for machine learning software: experiences from the scikit-learn project, 2013, http://dx.doi.org/10.48550/arXiv.1309.0238.
[51] A. Afzal, K.-Y. Kim, J.-w. Seo, Effects of latin hypercube sampling on surrogate modeling and optimization, Int. J. Fluid Mach. Syst. 10 (3) (2017) 240–253, http://dx.doi.org/10.5293/IJFMS.2017.10.3.240.
[52] M.D. Shields, J. Zhang, The generalization of latin hypercube sampling, Reliab. Eng. Syst. Saf. 148 (2016) 96–108, http://dx.doi.org/10.1016/j.ress.2015.12.002.
[53] C.D. Lin, B. Tang, Latin hypercubes and space-filling designs, 2022, http://dx.doi.org/10.48550/arXiv.2203.06334.
[54] M.D. McKay, R.J. Beckman, W.J. Conover, A comparison of three methods for selecting values of input variables in the analysis of output from a computer code, Technometrics 21 (2) (1979) 239, http://dx.doi.org/10.2307/1268522.
[55] D.E. Huntington, C.S. Lyrintzis, Improvements to and limitations of latin hypercube sampling, Probabilistic Eng. Mech. 13 (4) (1998) 245–253, http://dx.doi.org/10.1016/S0266-8920(97)00013-1.
[56] D.R. Jones, M. Schonlau, W.J. Welch, Efficient global optimization of expensive black-box functions, J. Global Optim. 13 (4) (1998) 455–492, http://dx.doi.org/10.1023/A:1008306431147.
[57] M. Han, Q. Huang, L. Ouyang, X. Zhao, A kriging-based active learning algorithm for contour estimation of integrated response with noise factors, Eng. Comput. 39 (2) (2023) 1341–1362, http://dx.doi.org/10.1007/s00366-021-01516-2.
[58] F. Yang, C.D. Lin, P. Ranjan, Global fitting of the response surface via estimating multiple contours of a simulator, 2019, URL http://arxiv.org/pdf/1902.01011v1.
[59] J. Schmeink, M. Schnoes, Automated Component Preliminary Design and Evaluation in the Overall Engine Using Fully Coupled Approaches. http://dx.doi.org/10.1115/GT2022-80634.
[60] V. Gnielinski, G1 heat transfer in pipe flow, in: VDI Heat Atlas, Springer Berlin Heidelberg, Berlin, Heidelberg, 2010, pp. 691–700, http://dx.doi.org/10.1007/978-3-540-77877-6_34.
[61] E.S. Gaddis, V. Gnielinski, G8 shell-side heat transfer in baffled shell-and-tube heat exchangers, in: VDI Heat Atlas, Springer Berlin Heidelberg, Berlin, Heidelberg, 2010, pp. 731–742, http://dx.doi.org/10.1007/978-3-540-77877-6_41.
[62] W. Kast, R. by Hermann Nirschl, E.S. Gaddis, K.-E. Wirth, J. Stichlmair, L1 pressure drop in single phase flow, 2010, URL https://api.semanticscholar.org/CorpusID:92853400.
[63] J.D. Denton, Throughflow calculations for transonic axial flow turbines, J. Eng. Power 100 (2) (1978) 212–218, http://dx.doi.org/10.1115/1.3446336, URL https://doi.org/10.1115/1.3446336.
[64] M. Schnös, Eine Auslegungsmethodik für mehrstufige Axialverdichter auf Basis einer Profildatenbank, Tech. rep., Ruhr-Universität Bochum, 2020, URL https://elib.dlr.de/140758/.